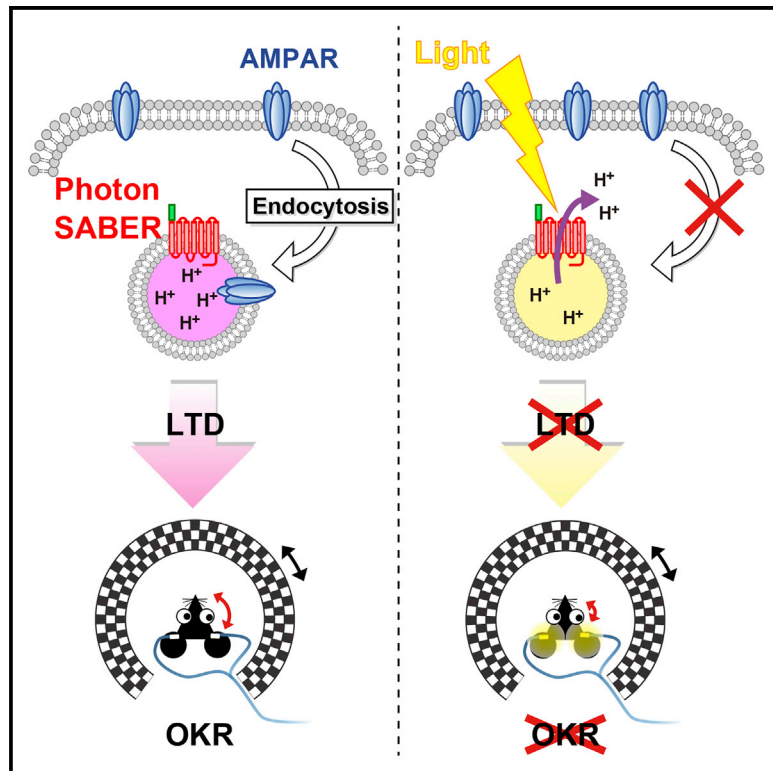# Optogenetic Control of Synaptic AMPA Receptor Endocytosis Reveals Roles of LTD in Motor Learning

Graphical Abstract

Authors

Wataru Kakegawa, Akira Katoh, Sakae Narumi, ..., Yugo Fukazawa, Michisuke Yuzaki, Shinji Matsuda

Correspondence

myuzaki@keio.jp (M.Y.),
smatsuda@uec.ac.jp (S.M.)

In Brief

Kakegawa et al. show that AMPA receptor endocytosis at parallel fiber-Purkinje cell synapses in the cerebellar flocculus plays a direct role in motor learning *in vivo*, using a new optogenetic tool, PhotonSABER, which enables the acute inhibition of AMPA receptor endocytosis during LTD.

Highlights

- A new optogenetic tool, PhotonSABER, controls endocytosis at active synapses

- PhotonSABER inhibits AMPA receptor endocytosis during LTD in a light-dependent manner

- Basal synaptic transmission and other forms of synaptic plasticity were unaffected

- PhotonSABER inhibits AMPA receptor endocytosis and motor learning in Purkinje cells *in vivo*

CellPress

Optogenetic Control of Synaptic AMPA Receptor Endocytosis Reveals Roles of LTD in Motor Learning

Wataru Kakegawa,[1] Akira Katoh,[2] Sakae Narumi,[3] Eriko Miura,[1] Junko Motohashi,[1] Akiyo Takahashi,[4] Kazuhisa Kohda,[3] Yugo Fukazawa,[5] Michisuke Yuzaki,[1,8,*] and Shinji Matsuda[1,4,6,7,*]

[1]Department of Physiology, Keio University School of Medicine, Tokyo 160-8582, Japan
[2]Department of Physiology, Tokai University School of Medicine, Kanagawa 259-1193, Japan
[3]Department of Physiology, St. Marianna University School of Medicine, Kanagawa 216-8511, Japan
[4]Department of Engineering Science, Graduate School of Informatics and Engineering, The University of Electro-Communications, Tokyo 182-8585, Japan
[5]Department of Anatomy, University of Fukui School of Medical Sciences, Fukui 910-1193, Japan
[6]Japan Science and Technology Agency, PRESTO, 4-1-8 Honcho Kawaguchi, Saitama 332-0012, Japan
[7]Brain Science Inspired Life Support Research Center (BLSC), The University of Electro-Communications, Tokyo 182-8585, Japan
[8]Lead Contact
*Correspondence: myuzaki@keio.jp (M.Y.), smatsuda@uec.ac.jp (S.M.)
https://doi.org/10.1016/j.neuron.2018.07.034

SUMMARY

Long-term depression (LTD) of AMPA-type glutamate receptor (AMPA receptor)-mediated synaptic transmission has been proposed as a cellular substrate for learning and memory. Although activity-induced AMPA receptor endocytosis is believed to underlie LTD, it remains largely unclear whether LTD and AMPA receptor endocytosis at specific synapses are causally linked to learning and memory *in vivo*. Here we developed a new optogenetic tool, termed PhotonSABER, which enabled the temporal, spatial, and cell-type-specific control of AMPA receptor endocytosis at active synapses, while the basal synaptic properties and other forms of synaptic plasticity were unaffected. We found that fiberoptic illumination to Purkinje cells expressing PhotonSABER *in vivo* inhibited cerebellar motor learning during adaptation of the horizontal optokinetic response and vestibulo-ocular reflex, as well as synaptic AMPA receptor decrease in the flocculus. Our results demonstrate that LTD and AMPA receptor endocytosis at specific neuronal circuits were directly responsible for motor learning *in vivo*.

INTRODUCTION

The cerebellum is an ideal brain region for the investigation of the association of synaptic plasticity at certain synapses with learning and memory processes *in vivo*, since it comprises relatively simple neuronal circuits and provides a direct link to motor outputs (De Zeeuw and Ten Brinke, 2015; Ito et al., 2014). Long-term depression of excitatory synaptic transmission at parallel fiber (PF)-Purkinje cell synapses (PF-LTD) in the cerebellar cortex has long been proposed as a basis of the motor learning

mechanism underlying visual adaptation of the horizontal optokinetic response (OKR) and vestibulo-ocular reflex (VOR), as well as eyeblink conditioning (Ito et al., 2014). Indeed, various genetically engineered mice with disruptions in the expression of key molecules necessary for PF-LTD induction *in vitro* display impaired motor learning *in vivo* (Ito et al., 2014; Yuzaki, 2013). Recently, however, three lines of genetically modified mice in which PF-LTD was impaired in slice preparations have been shown to display normal motor learning (Schonewille et al., 2011). Instead, long-term potentiation at PF-Purkinje cell synapses (PF-LTP) and rebound potentiation (RP) of inhibitory synaptic inputs to Purkinje cells have been proposed as alternative substrates for motor learning (Gutierrez-Castellanos et al., 2017; Schonewille et al., 2010; Tanaka et al., 2013). Similarly, a discrepancy between synaptic plasticity at the circuit level and learning at the behavioral level has been reported in the hippocampus (Martin and Morris, 2002). To resolve this issue, new tools for the direct and acute modification of synaptic plasticity at specific neuronal circuits *in vivo* are needed.

The discrepant LTD results are at least partly attributable to various LTD induction protocols used in *in vitro* slice preparations (Suvrathan et al., 2016; Yamaguchi et al., 2016). However, the final common step of LTD is believed to be the reduction of postsynaptic AMPA-type glutamate receptors (AMPA receptors) by activity-dependent, clathrin-mediated endocytosis (Collingridge et al., 2010; Huganir and Nicoll, 2013). For example, LTD is inhibited by disrupting AMPA receptor association with the clathrin adaptor protein AP-2 in hippocampal neurons (Matsuda et al., 2013) and Purkinje cells (Nomura et al., 2012). In addition, dominant-negative forms of Rab5 (Brown et al., 2005) or Rab7 (Fernández-Monreal et al., 2012), small G proteins necessary for endosomal trafficking (Segev, 2011), inhibit LTD in hippocampal neurons. As acidification of the endosomal lumen is essential for endocytosis (Kozik et al., 2013) and endosomal maturation (Huotari and Helenius, 2011), we developed a new optogenetic tool to regulate activity-dependent endocytosis by expressing a photosensitive proton (H$^+$) pump in endosomes. Using this
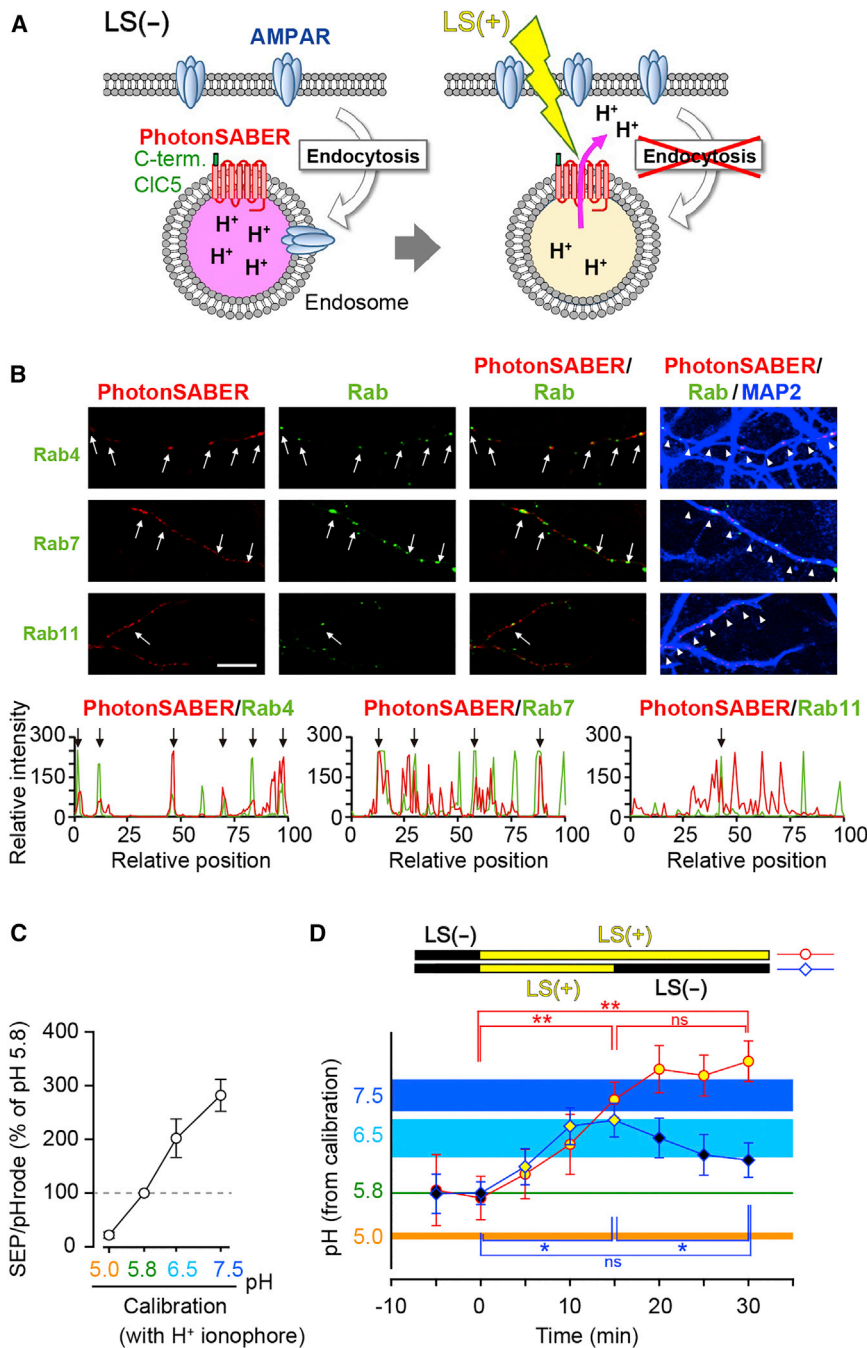
Figure 1. PhotonSABER Regulates Endosomal pH by Light Stimulation

(A) Schematic drawing of PhotonSABER. PhotonSABER de-acidifies the endosomal lumen through light-stimulated H^+ pump activities and inhibits the endocytosis of AMPA receptor (AMPAR). LS, light stimulation; ClC5, chloride channel protein 5.

(B) Distribution of PhotonSABER (red) and Rab-GFPs (green; top, Rab4; middle, Rab7; bottom, Rab11) in dendrites (blue, MAP2) in cultured hippocampal neurons. Scale bar, 10 μm. The lower line-scan graphs indicate the fluorescent intensities of PhotonSABER and Rab-GFP along dendrites marked by arrowheads. The arrows in the upper panels and line-scan graphs indicate PhotonSABER colocalized with Rab-GFPs.

(C) Calibration of endosomal pH in the dendrites of hippocampal neurons. Hippocampal neurons expressing SEP-tagged PhotonSABER were incubated with dextran-conjugated pHrode. The fluorescence ratios in the pH calibration buffers containing H^+-ionophore are shown. The average value at pH 5.8 was established as 100%. n = 6 endosomes from 6 neurons.

(D) Effect of continuous and transient illumination on endosomal pH. Time-lapse imaging was performed in dendrites of hippocampal neurons expressing PhotonSABER during 30 min of continuous (red circles) or 15 min of illumination followed by darkness (blue diamonds). n = 6–7 endosomes from 6 neurons for each time point. The y axis indicates the estimated endosomal pH with its range of errors (±SEM) based on the calibration (C). $**p < 0.01$ and $*p < 0.05$; ns, not significant. Data points represent mean ± SEM. See also Figure S1.

placed by Glu (ASR^{D217E}), which enables H^+ transport from the lumen to the cytosol via single-photon activation (Kawanabe et al., 2009). To target ASR^{D217E} to early endosomes and immunodetect its localization, we fused the C-terminal cytoplasmic region of chloride channel protein 5 (Schwake et al., 2001) and the FLAG tag to the ASR^{D217E} (Figure 1A). We named this construct PhotonSABER (photon-sensitive ASR-based endocytosis regulator), and we coexpressed it with GFP-tagged small G proteins in HEK293 cells and cultured hippocampal neurons. Immunocytochemical staining of FLAG revealed that PhotonSABER colocalized mostly with Rab4 (55% ± 4%, n = 8 cells) and Rab7 (57% ± 5%, n = 8 cells), compared with Rab11 (40% ± 4%, n = 8 cells, p = 0.038; ANOVA with a Bonferroni correction) in hippocampal neurons (arrows, Figure 1B) and HEK293 cells (Figure S1A). Because Rab7 and Rab11 target late and recycling endosomes, respectively (Segev, 2011), while Rab4 is present in early and recycling endosomes by linking Rab5- and Rab11-dependent pathways (Hoogenraad et al., 2010; Sönnichsen et al., 2000), these results indicate that

tool, we demonstrate that LTD and AMPA receptor endocytosis at PF-Purkinje cell synapses in the flocculus are directly responsible for the motor learning underlying OKR and VOR *in vivo*.

RESULTS

PhotonSABER Regulates Endosomal pH by Light Stimulation

To acutely de-acidify endosomal pH, we took advantage of an engineered *Anabaena* sensory rhodopsin in which Asp217 is re-

overexpressed PhotonSABER was mainly targeted to the early to late endosomes.

To examine if PhotonSABER can control the endosomal pH with light stimulation, we fused super-ecliptic pHluorin (SEP), a pH-sensitive GFP that emits less fluorescence in acidic environments (Miesenböck et al., 1998), to the luminal N-terminal region of PhotonSABER. To identify the endosomes and perform ratiometric measurement, HEK293 cells and hippocampal neurons expressing SEP-tagged PhotonSABER were incubated with a dextran-conjugated pH-sensitive red dye (pHrode) that increases fluorescence intensity in acidic endosomal compartments. Confocal microscopic imaging showed that the fluorescence ratio of SEP to pHrode in the endosomes increased with light stimulation in HEK293 cells (Figure S1B) and in the dendrites of hippocampal neurons (Figure 1C). The fluorescence ratio measured in various pH calibration buffers containing an H^+-ionophore indicated that the endosomal pH was elevated by $\sim$0.5 (Figure 1C; Figure S1B) following illumination for 10 min. Time-lapse imaging of the dendrites of hippocampal neurons showed that endosomal pH gradually increased with illumination over 30 min (p = 0.001 between t = 0 and 15 min; p = 0.130 between t = 15 and 30 min; p < 0.001 between t = 0 and 30 min; one-way ANOVA followed by Fisher's least significant difference [LSD] post hoc test, n = 6), but returned toward the near-basal level within $\sim$15 min after the cessation of illumination after 15 min (p = 0.075 between t = 0 and 30 min; p = 0.046 between t = 15 and 30 min, n = 7) (Figure 1D). We obtained essentially the same results with time-lapse imaging in COS-7 cells (Figure S1C). These time courses likely reflect the ASR^{D217E} kinetics (15.1 ± 4.0 H^+ ions/min/molecule) (Kawanabe et al., 2009) and the counteracting activity of vacuolar ATPase in endosomes. Together, these results demonstrate that PhotonSABER can rapidly and reversibly control endosomal pH in a light-dependent manner.

PhotonSABER Inhibits Endocytosis in a Light-Dependent Manner

To test the effect on endosomal trafficking, we expressed PhotonSABER together with Rab7-GFP in HEK293 cells and incubated them with biotinylated dextran for 1 hr with or without light stimulation. The amount of dextran in Rab7-positive late endosomes was significantly reduced by illumination (Figures S2A and S2B). Increasing light intensity further reduced dextran transport to late endosomes (Figure S2C), indicating that PhotonSABER inhibited endocytosis of dextran in a light-dependent manner.

We next examined the performance of PhotonSABER in cultured hippocampal neurons using a chemical LTD protocol with N-methyl-ᴅ-aspartate (NMDA) to induce AMPA receptor endocytosis. We expressed GluA2 AMPA receptor subunits with a hemagglutinin (HA)-tag attached to the extracellular N terminus (HA-GluA2) together with PhotonSABER in cultured hippocampal neurons. Immunocytochemical analyses showed that the expression of PhotonSABER did not affect the colocalization ratio of HA-GluA2 and mannose-6-phosphate receptor (M6PR; Figure S3A), a late endosomal marker (Griffiths et al., 1988), indicating that PhotonSABER does not interfere with basal late endosomal trafficking. Application of 50 μM NMDA for 10 min reduced surface HA-GluA2 under dark conditions

(p = 0.002, n = 11−12; Figures S3B and S3C, upper panels) (Lee et al., 2004; Matsuda et al., 2013). Although light stimulation did not affect the basal surface GluA2 levels in hippocampal neurons (dark, 100% ± 6%, n = 11 cells; light, 94% ± 6%, n = 12 cells; p = 0.50, two-tailed Student's t test), it inhibited the NMDA-induced reduction of cell surface HA-GluA2 (p = 0.49, n = 12; Figures S3B and S3C, lower panels).

To clarify the effect of PhotonSABER on AMPA receptor trafficking, HA-GluA2 and Rab4-GFP were coexpressed in cultured hippocampal neurons together with PhotonSABER. AMPA receptors were found localized in Rab4-positive early endosomes 3 min after NMDA treatment, as reported previously (Lee et al., 2004; Matsuda et al., 2013). However, light stimulation significantly reduced the amount of GluA2 signal on Rab4-positive endosomes (Figures S3D and S3E). Furthermore, when living hippocampal neurons expressing HA-GluA2 were incubated with an anti-HA antibody, treated with NMDA for 3 min, and then fixed, the internalized anti-HA antibody-GluA2 complex was detected under the dark, but not the light, conditions (Figures S3F and S3G). These results indicate that PhotonSABER inhibited NMDA-induced AMPA receptor endocytosis by regulating early endosomal function in hippocampal neurons.

To characterize the illumination conditions necessary for the regulation of AMPA receptor endocytosis, we varied the wavelength using band-pass filters. While green (center wavelength/full width at half maximum, 542/27 nm) and yellow (575/25 nm) light inhibited AMPA receptor endocytosis in hippocampal neurons expressing PhotonSABER, the inhibitory effect was not observed with cyan (475/28 nm) or infrared (850/50 nm) light (Figure S4A). These results are consistent with the absorption spectrum and the action spectrum for the H^+ transport activity of ASR^{D217E}, both of which show a peak at $\sim$540 nm (Kawanabe et al., 2009). The inhibitory effect on AMPA receptor endocytosis was also dependent on light intensity and saturated at $\sim$1,000 lux (Figure S4B), a condition similar to dextran endocytosis in HEK293 cells (Figure S2C). Interestingly, focal light stimulation did not inhibit NMDA-induced reduction of surface HA-GluA2 in either the light-stimulated or unstimulated dendrites (Figures S5A and S5B), likely reflecting the highly dynamic nature of endosomes within neurons (Kerr and Teasdale, 2014). These results indicate that the effect of PhotonSABER on the surface HA-GluA2 was dependent on the conditions of light stimulation.

Finally, we examined the performance of PhotonSABER in cultured Purkinje cells. We induced chemical LTD in Purkinje cells (Matsuda et al., 2000; Xia et al., 2000) expressing HA-GluA2 and PhotonSABER by applying 1 μM phorbol 12-myristate 13-acetate (TPA), a potent protein kinase C activator, for 20 min. Immunocytochemical analyses revealed that the amount of cell surface GluA2 was significantly reduced by the TPA treatment under dark conditions (100% ± 8.2% without TPA treatment, n = 13 and 65.6% ± 5.9% with TPA treatment, n = 11; p = 0.046; Figures 2A, upper panels, and 2B). Although light stimulation did not affect the basal surface GluA2 levels in Purkinje cells (dark, 100% ± 8%, n = 13 cells; light, 114% ± 11%, n = 18 cells; p = 0.75, Kruskal-Wallis followed by Steel post hoc test), it significantly inhibited the effect of TPA on cell surface AMPA receptors (114% ± 11% without TPA treatment,
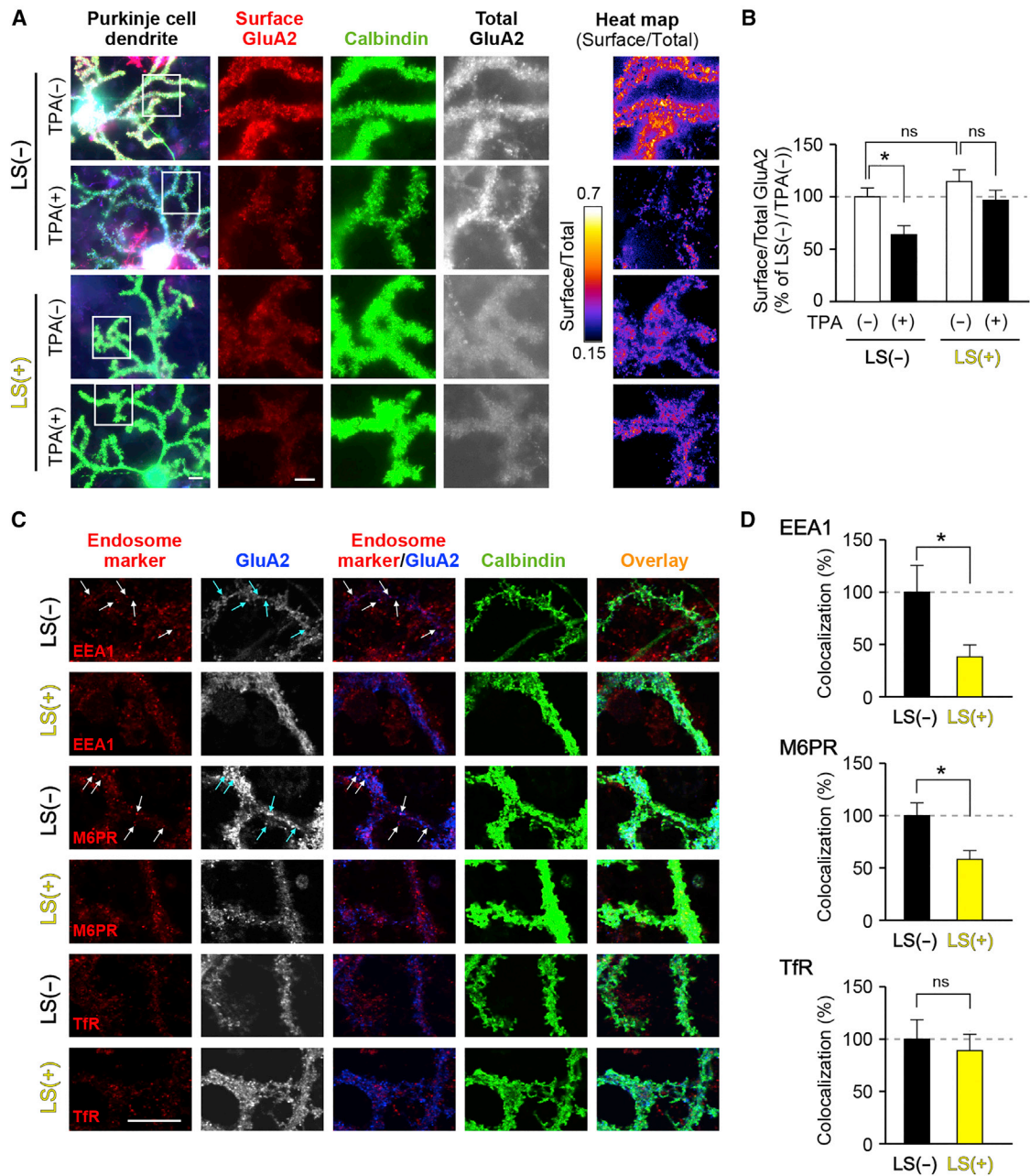
Figure 2. PhotonSABER Inhibits Chemical LTD in a Light-Dependent Manner

(A) Effects of PhotonSABER on chemical LTD in Purkinje cells. Cultured Purkinje cells expressing HA-GluA2 and PhotonSABER-FLAG were treated with 1 μM TPA for 20 min under dark (LS[−]) and light (LS[+]) conditions. Cells were immunostained for surface (red), total (blue or gray) HA-GluA2, and Calbindin (Purkinje cell marker, green). The regions marked by squares are magnified in the right panels. The ratio of the surface to total GluA2 fluorescence intensities is shown in the heatmaps. Scale bar, 10 μm.

(B) Quantification of TPA-induced changes in the ratio of surface to total GluA2 fluorescence intensities with (LS[+]) or without (LS[−]) light stimulation. The ratio in TPA-untreated neurons (LS[−]) was defined as 100% (n = 11−18 cells each). *p < 0.05; ns, not significant; Kruskal-Wallis test followed by Steel post hoc test. Data are presented as mean + SEM.

(C) Light stimulation decreased the colocalization of GluA2 with early and late endosomes. Purkinje cells expressing HA-GluA2 and PhotonSABER were treated with 1 μM TPA for 3 min (for EEA1 and TfR) or 20 min (for M6PR). Cells were co-immunostained for Calbindin (green); HA-GluA2 (blue); and markers for early (EEA1), late (M6PR), and recycling (TfR) endosomes (red). Arrows indicate double-immunopositive puncta for HA-GluA2 and endosomal markers. Scale bar, 10 μm.

(D) Quantitative analysis of GluA2 immunoreactivity colocalized with EEA1-, M6PR-, and TfR-positive endosomes with (LS[+]) or without (LS[−]) light stimulation. The average value under dark conditions was defined as 100%. n = 7−9 cells from 2 independent experiments.

**p < 0.01 and *p < 0.05; ns, not significant; two-tailed Student's t test. Data are presented as mean + SEM. See also Figures S2–S5.

n = 18 and 96% ± 10% with TPA treatment, n = 17; p = 0.76 and p = 0.99, respectively, versus basal surface GluA2 levels in dark conditions; Figures 2A and 2B).

To clarify the underlying mechanism without relying on ectopically expressed Rab proteins, we examined the colocalization of HA-GluA2 with endosomes using antibodies against early (early endosome antigen 1 [EEA1]), late (M6PR), and recycling (transferrin receptor [TfR]) endosomes in Purkinje cells after chemical LTD induction. We found that light stimulation significantly reduced the amount of HA-GluA2 signals on EEA1- and M6PR-positive endosomes, but not on TfR-positive endosomes (Figures 2C and 2D), indicating that PhotonSABER inhibits AMPA receptor trafficking to early and late endosomes in Purkinje cells. Together, these results verify that PhotonSABER inhibits the AMPA receptor internalization that is induced by chemical LTD in both hippocampal and Purkinje cells by light-dependent inhibition of endocytosis.

Generation and Characterization of PC-PhotonSABER Mice

The above data indicated that PhotonSABER could be a powerful tool to investigate the *in vivo* roles of LTD in modulating forms of learning and memory. To achieve cell-type-specific expression and to avoid problems associated with virus-mediated overexpression of exogenous proteins, we generated mice in which a cDNA encoding a stop signal flanked by *loxP* sites (*LSL*) followed by HA-tagged PhotonSABER was knocked in to the ROSA26 locus (*PhotonSABER-LSL*; control mice) (Figure 3A). Because the role of PF-LTD in cerebellar learning remains controversial, we crossed *PhotonSABER-LSL* mice with *L7-Cre* mice, which specifically expressed *Cre* in Purkinje cells. Immunoblot analyses confirmed the specific expression of PhotonSABER-HA proteins in the cerebellar lysates from *PhotonSABER-LSL;L7-Cre* (PC-PhotonSABER) mice (Figure 3B). Immunohistochemical analyses of cerebellar slices from PC-PhotonSABER mice revealed that HA immunoreactivity was selectively found in Purkinje cells (Figure 3C) and predominantly colocalized with EEA1 and M6PR and to a lesser extent with TfR, and not with lysosomal-associated membrane protein 1 (LAMP1, a lysosomal marker; Figures 3D and 3E), indicating that PhotonSABER was mainly localized in early to late endosomes *in vivo*.

We examined the basic properties of Purkinje cells using whole-cell patch-clamp recordings in acute slice preparations from the vermis of PC-PhotonSABER and control mice under dark conditions. We did not observe any difference in spontaneous spike frequency (Figure S6A) or membrane resistance and capacitance (Figure S6B) between the control and PC-PhotonSABER slices. Similarly, the amplitude and frequency of miniature excitatory postsynaptic currents (mEPSCs) were similar between the control and PC-PhotonSABER slices (Figure S6C). These results indicate that expression of PhotonSABER itself does not affect the basic electrophysiological properties of Purkinje cells.

Next, we recorded PF-evoked and climbing fiber (CF)-evoked EPSCs in PC-PhotonSABER mice under dark and light conditions. The amplitudes of PF- and CF-EPSCs were not affected by illumination (Figures 4A and 4B). Similarly, the paired-pulse ratio of PF- and CF-EPSCs, which reflects presynaptic functions (Zucker and Regehr, 2002), was unaffected by illumination (Figures 4A and 4B). Together, these results indicate that PhotonSABER does not affect basal AMPA receptor trafficking with or without light stimulation, a finding consistent with earlier reports that AMPA receptors do not undergo rapid recycling under basal conditions (Kakegawa and Yuzaki, 2005; Lee et al., 2002).

PF-LTD, but Not PF-LTP or RP, Is Impaired in the PC-PhotonSABER Cerebellum

We next examined various synaptic plasticity models in slices prepared from the vermis of PC-PhotonSABER mice. While conjunctive stimulation (CJ-stim) of PFs and direct depolarization of Purkinje cells (30 pairs at 1 Hz) induced robust PF-LTD under dark conditions (0.70 ± 0.02 at 25−30 min after CJ-stim, n = 10; Figure 4C), PF-LTD was not induced under light conditions (0.93 ± 0.03 at 25−30 min after CJ-stim, n = 9; p = 0.0003, Mann-Whitney U test; Figure 4C). After confirming that CJ-stim failed to induce LTD under light conditions (Wilcoxon signed-rank test, p = 0.398 at EPSC amplitudes between 1 min before and 30 min after first CJ-stim; Figure 4D), slices were kept in the dark condition for 10 min, and then the same CJ-stim (second CJ-stim) was applied. We found robust LTD induction in these slices (0.73 ± 0.03 at 25–30 min after second CJ-stim, n = 7; Wilcoxon signed-rank test, p = 0.018 at EPSC amplitudes between 1 min before and 30 min after second CJ-stim; Figure 4D), indicating that the perturbation of AMPA receptor endocytosis is reversible. When light stimulation was applied to cerebellar slices 30 min after the induction of PF-LTD, PF-EPSC did not show further changes (0.71 ± 0.03 at 30 min and 0.71 ± 0.04 at 55 min after CJ-stim, n = 7; p = 0.735, Wilcoxon signed-rank test; Figure 4E). These results are consistent with earlier studies showing that AMPA receptors are transported beyond late endosomes after 30 min of LTD induction (Lee et al., 2004; Matsuda et al., 2013), and they indicate that activation of PhotonSABER specifically inhibited the induction, but not the maintenance, of PF-LTD.

In contrast, PF-LTP, which could be induced by 1-Hz stimulation of PFs in current-clamp mode, was unaffected by light stimulation (dark, 1.26 ± 0.08 at 30−35 min after LTP-inducing stimulation, n = 5; light, 1.30 ± 0.13 at 30−35 min after LTP-inducing stimulation, n = 6; p = 0.855, Mann-Whitney U test; Figure 4F). Furthermore, illumination did not affect the RP of inhibitory postsynaptic currents (dark, 1.28 ± 0.08 at t = 30 min after RP-inducing stimulation, n = 7; light, 1.27 ± 0.15 at t = 30 min after RP-inducing stimulation, n = 8; p = 0.189, Mann-Whitney U test; Figure 4G), indicating that synaptic plasticity at the inhibitory inputs to Purkinje cells is unaffected by illumination (Tanaka et al., 2013). Together, these results indicate that PF-LTD induction is selectively and reversibly controlled with light in PC-PhotonSABER mice.

Because the flocculus is responsible for OKR and VOR (De Zeeuw and Ten Brinke, 2015; Ito et al., 2014), we next examined PF-LTD and PF-LTP in slices prepared from the flocculus (Figure 5A). As observed in slices from the vermis, we found that light stimulation specifically inhibited the induction of PF-LTD (dark, 0.69 ± 0.02 at 25−30 min after CJ-stim, n = 7; light,
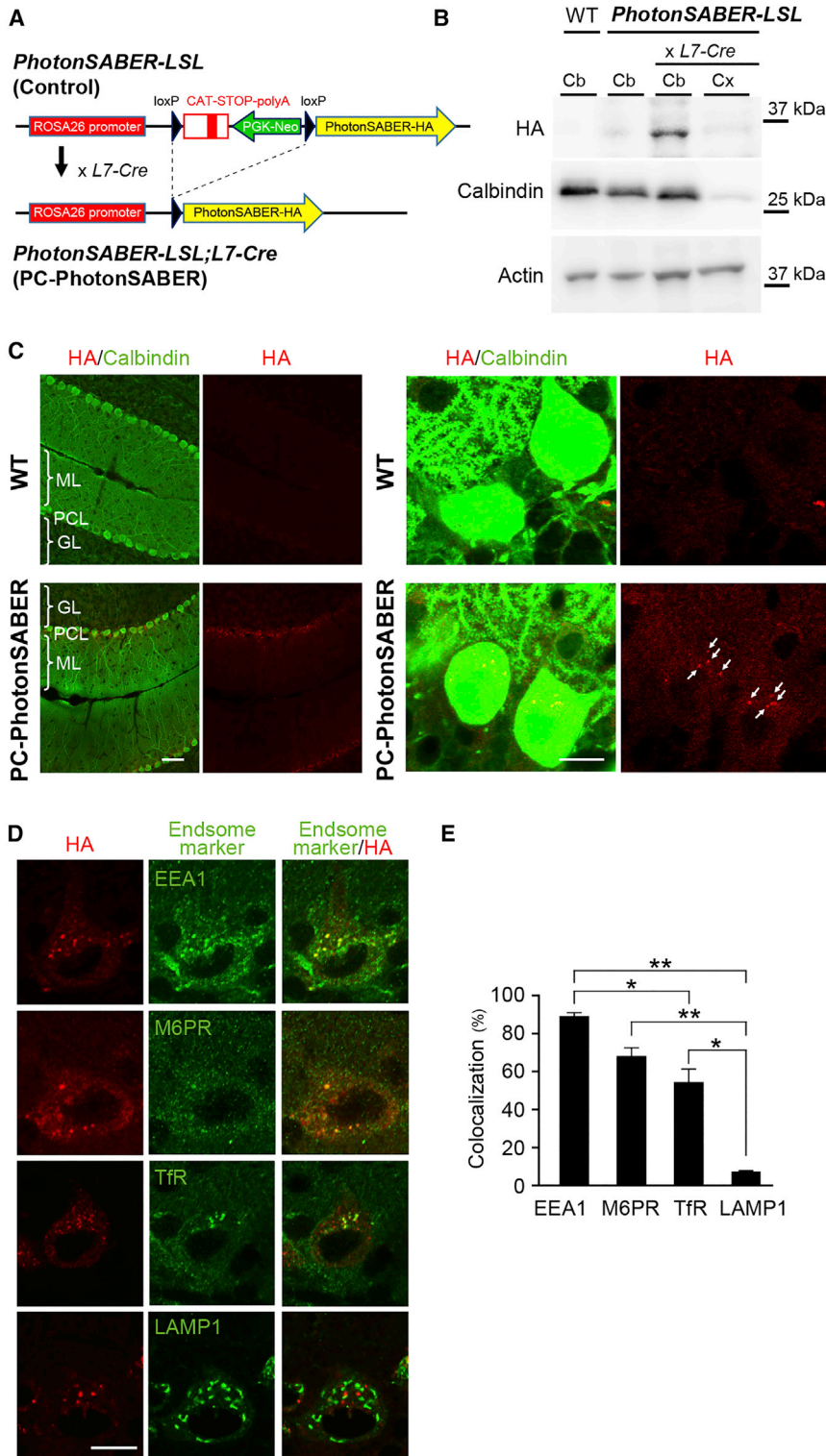
Figure 3. Generation of the Purkinje Cell-Specific PhotonSABER Mouse

(A) Schematic representation of *PhotonSABER-LSL;L7-Cre* knockin mice. The cDNAs encoding chloramphenicol acetyltransferase (*CAT*) and phosphoglycerate kinase I-neomycin resistance gene (PGK-*Neo*) were flanked by two *loxP* sites (*LSL*) in the reverse direction. The *LSL* cassette, followed by PhotonSABER-HA, was knocked into the ROSA26 locus to generate *PhotonSABER-LSL* mice (top, control mice). *PhotonSABER-LSL* mice were crossed with *L7-Cre* mice to generate *PhotonSABER-LSL;L7-Cre* (PC-PhotonSABER) mice (bottom).

(B) Immunoblot analysis of lysates of the cerebellum (Cb) and cerebral cortex (Cx) from wild-type (WT), *PhotonSABER-LSL*, and PC-PhotonSABER mice probed with anti-HA, anti-Calbindin-D28K, and anti-actin antibodies.

(C) Immunohistochemical analyses of the cerebellum from wild-type (WT, top) and PC-PhotonSABER (bottom) mice using anti-HA and anti-Calbindin-D28K antibodies. PhotonSABER-HA immunoreactivities were observed in the Purkinje cell layer (PCL) and molecular layer (ML) of PC-PhotonSABER mice. GL, granular layer. The right panels show the magnified images. Arrows indicate punctate PhotonSABER-HA immunoreactivities in Purkinje cell bodies. Scale bars, 50 μm (left) and 10 μm (right).

(D) Immunohistochemical analyses of the localization of PhotonSABER. The cerebellum of PC-PhotonSABER mouse was immunostained for HA, endosome markers (EEA1 for early endosomes, M6PR for late endosomes, and TfR for recycling endosomes), and LAMP1 as a lysosomal maker. Scale bar, 10 μm.

(E) Quantitative analysis of PhotonSABER-HA immunoreactivity colocalized with EEA1-, M6PR-, and TfR-positive endosomes and LAMP1-positive lysosomes. n = 10−14 cells from 2 mice. **$p < 0.01$ and *$p < 0.05$, Kruskal-Wallis test followed by Scheffe post hoc test. Data are presented as mean + SEM.

$p = 0.700$, Mann-Whitney U test; Figure 5C). Interestingly, the inhibition of PF-LTD with light stimulation was faster in slices from the flocculus (Figure 5B) than from the vermis (Figures 4C and 4D). In the flocculus, which belongs to the zebrin-positive band, the stimulus that induces PF-LTD in the vermis can lead to AMPA receptor exocytosis and PF-LTP (De Zeeuw and Ten Brinke, 2015; Suvrathan et al., 2016; Wadiche and Jahr, 2005). Thus, it is possible that the potentiation pathway, which is partially activated by the LTD-inducing stimulus but masked by the robust depression pathway under the normal condition, may contribute to the faster recovery of PF-EPSCs when the depression pathway was inhibited by PhotonSABER. In addition,

0.92 ± 0.07 at 25−30 min after CJ-stim, n = 7; p = 0.007, Mann-Whitney U test; Figure 5B), but not PF-LTP (dark, 1.44 ± 0.09 at t = 30−35 min after LTP-inducing stimulation, n = 6; light, 1.39 ± 0.13 at 30−35 min after LTP-inducing stimulation, n = 6;
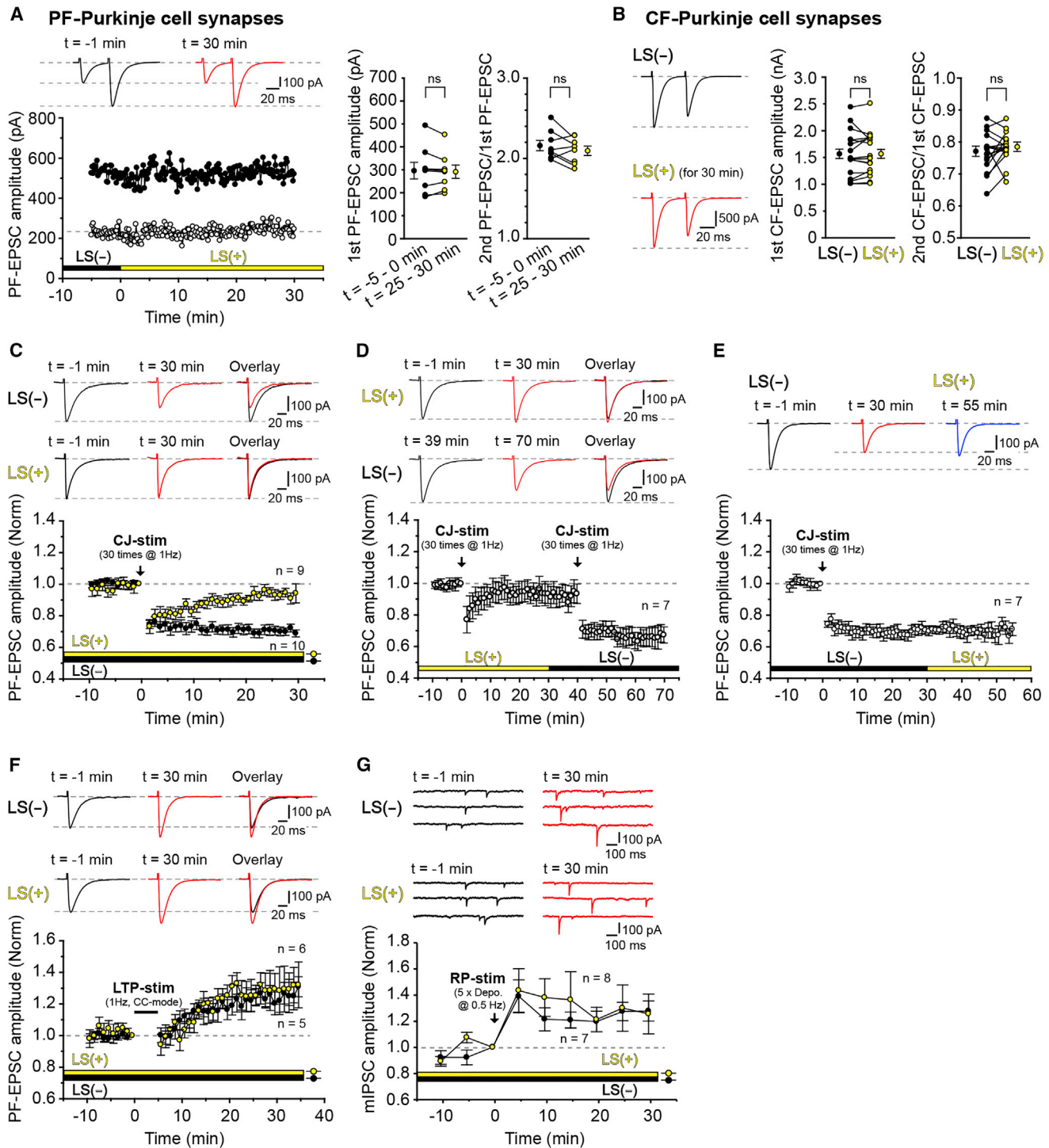
Vermis

Figure 4. Light Stimulus Impairs PF-LTD, but Not PF-LTP or RP, in the Vermis of PC-PhotonSABER Mice

(A) Light stimulus (LS) does not affect basal synaptic transmission at PF-Purkinje cell synapses. PFs were stimulated with paired-pulses (50-ms interstimulus interval) to evaluate the presynaptic functions in cerebellar slices from PC-PhotonSABER mice. The traces indicate representative PF-EPSCs −1 min (left) and 30 min (red, right) after LS. The lower graph shows the amplitudes of the first (open circles) and second (filled circles) PF-EPSCs plotted against time. The right graphs show the changes (from t = −5−0 to t = 25−30 min) in the averaged amplitudes of the first PF-EPCSs (left) and the ratio of the second to the first PF-EPSCs (right). n = 8 cells from 5 slices in 3 mice.

the kinetics of LTD blockade are affected by changes in presynaptic release probability caused by endocannabinoid-dependent (Kreitzer and Regehr, 2001) and -independent (Crepel, 2007) pathways. To test these possibilities, we used botulinum neurotoxin light chain (BoNT^{LC}, 100 nM) in the patch pipette to block PF-LTP (Kakegawa and Yuzaki, 2005) during LTD recordings. We found that, in the presence of BoNT^{LC}, the time course of LTD blockade by PhotonSABER in the flocculus became much slower but had no effect on the presynaptic release probabilities (Figures 5D and 5E). These results indicate that the apparently faster kinetics of LTD blockade by PhotonSABER were at least partly caused by co-activation of the potentiation pathway in the flocculus.

Light Stimulus Inhibits Oculomotor Learning and AMPA Receptor Endocytosis

Using PC-PhotonSABER mice, we examined whether cerebellum-dependent motor learning tasks, such as the adaptation of OKR and VOR, were regulated by AMPA receptor endocytosis. To induce OKR, a checked-pattern screen was repeatedly moved in a horizontal direction (15 degrees) in front of the mice, which had optic fibers placed above the bilateral flocculi (Figure 6A). PC-PhotonSABER and control mice showed essentially the same basal OKR across different sinusoidal oscillation frequencies without fiberoptic illumination (Figure 6B). However, while 60 min of training at 0.33 Hz increased the OKR gain without light stimulation, the gain increase was significantly impaired with light stimulation (gain at 60 min, 0.47 ± 0.05, n = 21 with light stimulation and 0.80 ± 0.04, n = 13 without light stimulation; p < 0.001, two-way ANOVA; Figure 6C). When fiberoptic illumination was started 20 min after the end of the 60-min training in dark conditions, the OKR gain did not decrease during subsequent training (0.78 ± 0.06 at 60 min and 0.86 ± 0.04 at 150 min, n = 8; p = 0.037, Wilcoxon signed-rank test; Figure 6D). When we placed

optic fibers above the vermis, fiberoptic illumination did not affect the OKR adaptation in PhotonSABER-PC mice (gain at 60 min, 0.77 ± 0.05, n = 8; p > 0.05 with flocculus-unilluminated mice, two-way ANOVA; Figure 6E). Together, these results indicate that fiberoptic illumination to the flocculus specifically inhibited OKR adaptation.

Next, we examined the effect of PhotonSABER on the visual adaptation of the VOR using two protocols. In the gain-up protocol, the optokinetic stimulus was moved in the opposite direction from the head for 60 min of training (Figure 7A). The increase in the VOR gain observed with 30- and 60-min training was severely inhibited by fiberoptic illumination to the flocculus (p = 0.006 at 30 min and p = 0.009 at 60 min, two-way ANOVA followed by Bonferroni post hoc test; Figures 7B and 7C). In contrast, in the gain-down protocol, the optokinetic stimulus was moved in the same direction as the head for 60 min of training (Figure 7D). In both the illuminated and unilluminated PC-PhotonSABER mice, the VOR gain similarly decreased with 30- and 60-min training (p = 0.299, two-way ANOVA; Figures 7E and 7F). These results indicate that light stimulation to the flocculus of PhotonSABER mice specifically inhibited the adaptation of VOR in the gain-up, but not the gain-down, protocol.

Finally, to confirm the effect of PhotonSABER on AMPA receptor endocytosis in vivo during OKR adaptation (Figure 8A), we examined the density of AMPA receptors in the flocculus using quantitative and highly sensitive SDS-digested freeze-fracture replica labeling (SDS-FRL) (Masugi-Tokita and Shigemoto, 2007). Although a small fraction of the synapses were likely modified after learning in vivo, the SDS-FRL method (Chen et al., 2014) and biochemical assays (Padmashri et al., 2013; Tukey et al., 2013) have been shown to detect changes in postsynaptic AMPA receptors. We found that the density of AMPA receptors decreased at PF-Purkinje cell synapses after 60 min of training with OKR (p = 0.001, Kruskal-Wallis test followed by

(B) LS does not affect basal synaptic transmission at CF-Purkinje cell synapses. CFs were stimulated by paired pulses (50-ms interstimulus interval) to evaluate the presynaptic functions in the cerebellar slices from PC-PhotonSABER mice. The traces indicate representative CF-EPSCs −1 min (top trace) and 30 min (red, bottom trace) after LS. The right graphs show the changes (from t = −1−0 to t = 29−30 min) in the averaged amplitudes of the first CF-EPCSs (left) and the ratio of the second to the first CF-EPSCs (right). n = 17 cells from 5 slices in 3 mice.

(C) LS inhibits PF-LTD induction in the vermis. Traces indicate PF-EPSCs recorded from PC-PhotonSABER Purkinje cells with (LS[+]) and without (LS[−]) LS. Left and middle traces indicate PF-EPSCs −1 min before and at 30 min after conjunctive stimulations (CJ-stim; 30 × [single PF stimulation + Purkinje cell depolarization] at 1 Hz). Superimposed traces are also indicated in right panels. The lower graph indicates the quantitative analysis of the PF-EPSC amplitude. The amplitudes are normalized to the average EPSC amplitudes before CJ-stim. n = 10 cells from 10 slices in 6 mice in LS(−) and n = 9 cells from 9 slices in 6 mice in LS(+) conditions.

(D) Reversible effects of LS on PF-LTD induction. When CJ-stim was applied 10 min after the cessation of LS, PF-LTD was normally induced. Left and middle traces indicate PF-EPSCs −1 min before (t = −1 or 39 min) and at 30 min after (t = 30 or 70 min) each CJ-stim. Superimposed traces are also indicated in right panels. The lower graph indicates the quantitative analysis of the PF-EPSC amplitude. The amplitudes are normalized with average EPSC amplitudes before first CJ-stim. n = 7 cells from 7 slices in 7 mice.

(E) Effects of LS on PF-LTD maintenance. 30 min after LTD was induced under dark conditions, LS was applied to PC-PhotonSABER Purkinje cells. The traces indicate the PF-EPSC −1 min before and 30 and 55 min after CJ-stim. The lower graph indicates the quantitative analysis of the PF-EPSC amplitude. n = 7 cells from 7 slices in 6 mice.

(F) LS does not affect PF-LTP. The traces indicate PF-EPSCs −1 min before and 30 min after LTP-inducing stimulations (LTP-stim; 300 PF stimuli at 1 Hz in current-clamp mode) together with the superimposed traces (right). The lower graph indicates the quantitative analysis of the PF-EPSC amplitude. The amplitudes are normalized to the average EPSC amplitudes before LTP-stim. n = 5 cells from 5 slices in 4 mice in LS(−) and n = 6 cells from 6 slices in 6 mice in LS(+) conditions.

(G) LS does not affect RP. Representative miniature inhibitory postsynaptic current (mIPSC) traces are shown under LS(−) (top traces) and LS(+) (bottom traces) conditions in acute Purkinje cell slices prepared from PC-PhotonSABER mice. In both conditions, depolarization of Purkinje cells 5 times at 0.5 Hz (RP-stim) induced the RP of mIPSCs (right red traces). The bottom graph indicates the quantitative analysis of the mIPSC amplitude, which was normalized to the average mIPSC amplitude before RP induction. n = 7 cells from 7 slices in 5 mice in LS(−) and n = 8 cells from 8 slices in 5 mice in LS(+) conditions.

ns, not significant; Wilcoxon signed-rank test. Data are presented as mean ± SEM. See also Figures S6 and S7.
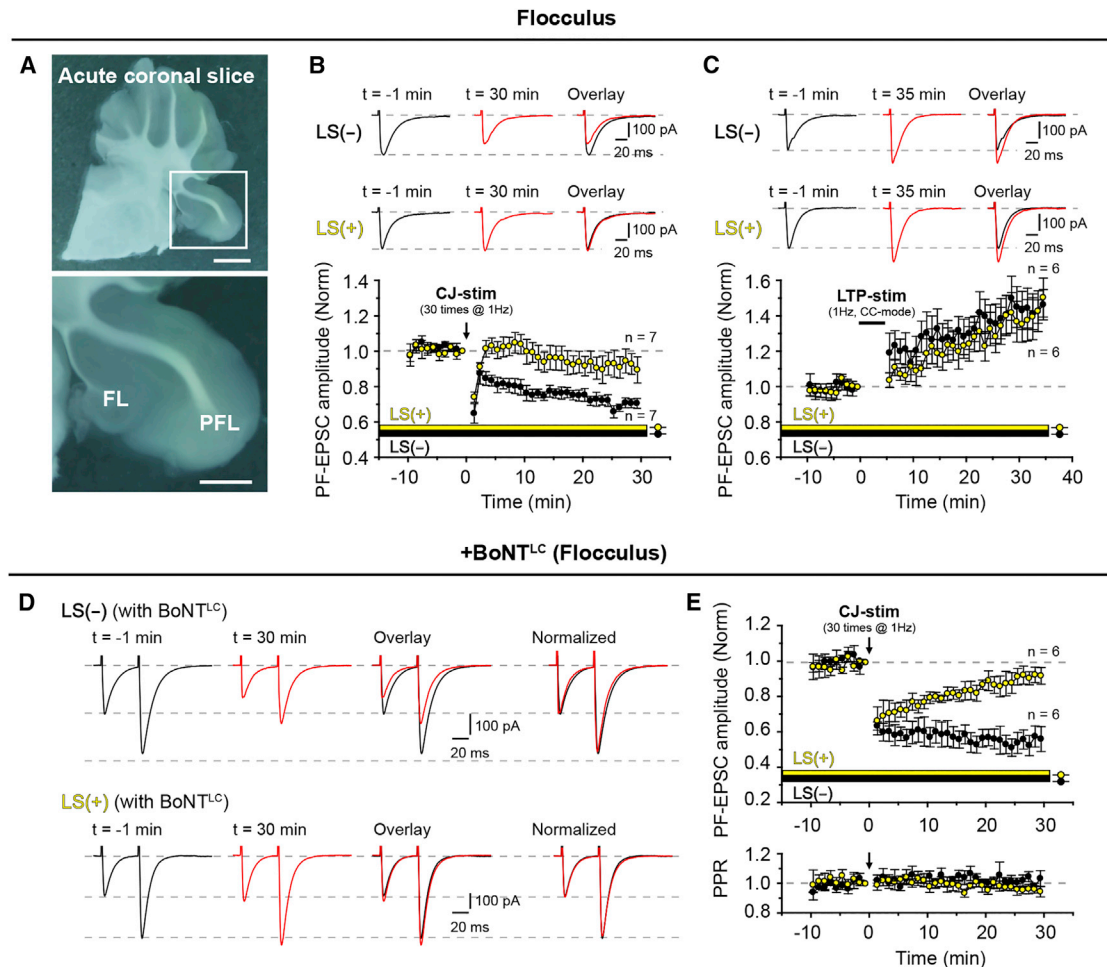
Flocculus

+BoNT^LC (Flocculus)

Figure 5. Light Stimulus Impairs PF-LTD, but Not PF-LTP, in the Flocculus of PC-PhotonSABER Mice

(A) The location of the flocculus (FL) and paraflocculus (PFL) in a coronal section of acute cerebellar slice. Scale bars, 1 mm (top) and 0.5 mm (bottom).

(B) Light stimulation (LS) impairs PF-LTD induction in the FL of PC-PhotonSABER mice. The upper traces indicate the PF-EPSCs recorded from Purkinje cells under dark (LS[−]) and light (LS[+]) conditions. The left and middle traces indicate the PF-EPSC −1 min before (left) and 30 min after (middle) conjunctive stimulation (CJ-stim). The superimposed traces are also shown in the right panels. The lower graph indicates the quantitative analysis of the PF-EPSC amplitude. The amplitudes were normalized to the average EPSC amplitudes before CJ-stim. CJ-stim induced a prolonged reduction of PF-EPSC amplitude under LS(−), but not LS(+), condition. n = 7 cells from 7 slices in 4 mice for each condition.

(C) LS did not affect LTP induction in the FL of PC-PhotonSABER mice. The upper traces indicate the PF-EPSC under LS(−) and LS(+) conditions. The traces indicate the PF-EPSC −1 min before (left) and 30 min after (middle) LTP-inducing stimulations (LTP-stim, 300 times of PF stimulation at 1 Hz under current clamp-mode) together with the superimposed traces (right). The lower graph indicates the quantitative analysis of the PF-EPSC amplitude. The amplitudes were normalized to the average EPSC amplitudes before LTP-stim. LTP-stim induced prolonged potentiation of the PF-EPSC amplitude under both LS(−) and LS(+) conditions. n = 6 cells from 6 slices in 5 mice for each condition.

(D) A slower time course of PF-LTD blockade by PhotonSABER in the absence of PF-LTP. The light chain of botulinum neurotoxin (BoNT^LC, 100 nM) was applied to Purkinje cells through the patch pipette to block PF-LTP during the PF-LTD recording. Paired-pulse stimulations (50-ms interstimulus interval) were applied to PFs to monitor the changes in the presynaptic release probability. The traces indicate the PF-EPSCs −1 min before (left) and 30 min after (middle) CJ-stim in LS(−) (upper traces) and LS(+) (lower traces) conditions. The superimposed traces and traces normalized with first EPSC amplitude are shown in the right panels.

(E) The quantitative analysis of the PF-EPSC amplitude in the presence of BoNT^LC. The amplitudes were normalized to the average EPSC amplitudes before CJ-stim. The bottom graph indicates the paired-pulse ratio of PF-EPSC. n = 6 cells from 6 slices in 6 mice for each condition. Data are presented as mean ± SEM.

Scheffe post hoc test; Figures 8B–8D), as reported previously (Wang et al., 2014). However, the OKR-induced decrease in AMPA receptors was inhibited with fiberoptic illumination (p = 0.984, Kruskal-Wallis test followed by Scheffe post hoc test; Figures 8B–8D). These results indicate that AMPA receptor endocytosis at PF-Purkinje cell synapses plays a direct role in OKR motor learning.

DISCUSSION

In the present study, we developed a new optogenetic tool, PhotonSABER, which enabled the temporal and reversible inhibition of early endosomal functions (Figures 1 and 2). Using PC-PhotonSABER knockin mice (Figure 3), we showed that light stimulation inhibited the induction of PF-LTD (Figures 4C and
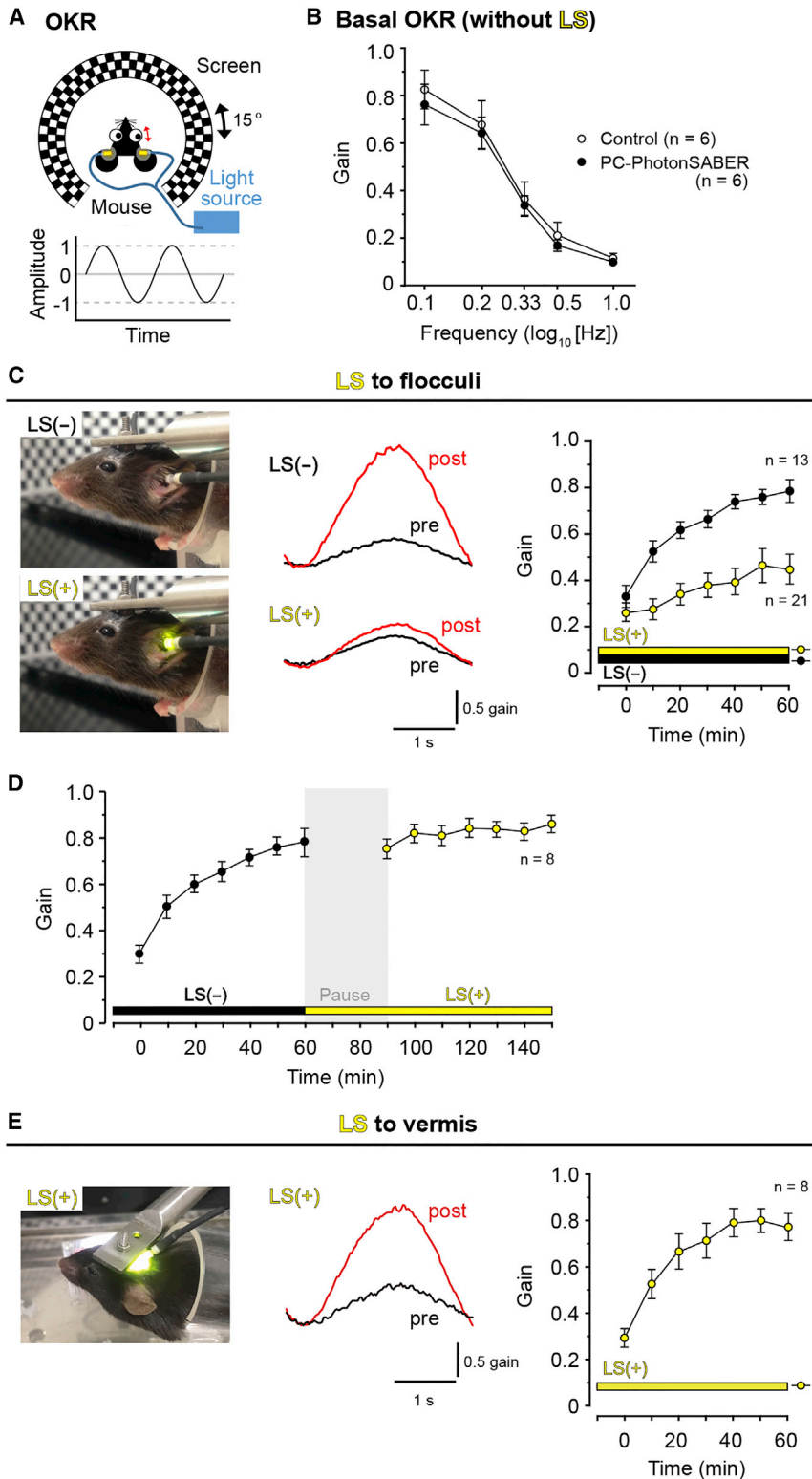
Figure 6. Fiberoptic Illumination Inhibits OKR Adaptation in PC-PhotonSABER Mice

(A) Schematic drawing of the experimental setup. The PC-PhotonSABER mouse, which had optic fibers placed above the bilateral flocculi, was surrounded by a checked-pattern screen. The eye movements made during sinusoidal oscillation of the screen (15 degrees) were monitored.

(B) Basal OKR across different sinusoidal oscillation frequencies. Without fiberoptic illumination (LS[–]), the PC-PhotonSABER and *PhotonSABER-LSL* (control) mice showed essentially the same basal OKR.

(C) Fiberoptic illumination to the bilateral flocculi inhibits OKR adaptation. The left traces indicate the representative OKR waveforms before (pre, black) and 60 min after (post, red) training without (LS[–]) and with (LS[+]) illumination. The right graph shows the time course of OKR adaptation (gain) under LS(–) (n = 13 mice) and LS(+) (n = 21 mice) conditions.

(D) Delayed illumination, which started 20 min after the end of the 60-min training in the LS(–) condition, did not affect the OKR gain. n = 8 mice.

(E) Fiberoptic illumination to the vermis does not affect OKR adaptation. The left traces indicate the representative OKR waveforms before (pre, black) and 60 min after (post, red) training with illumination (LS[+]) to the vermis. The right graph shows the time course of OKR adaptation (gain) with illumination (LS[+]) to the vermis. n = 8 mice.
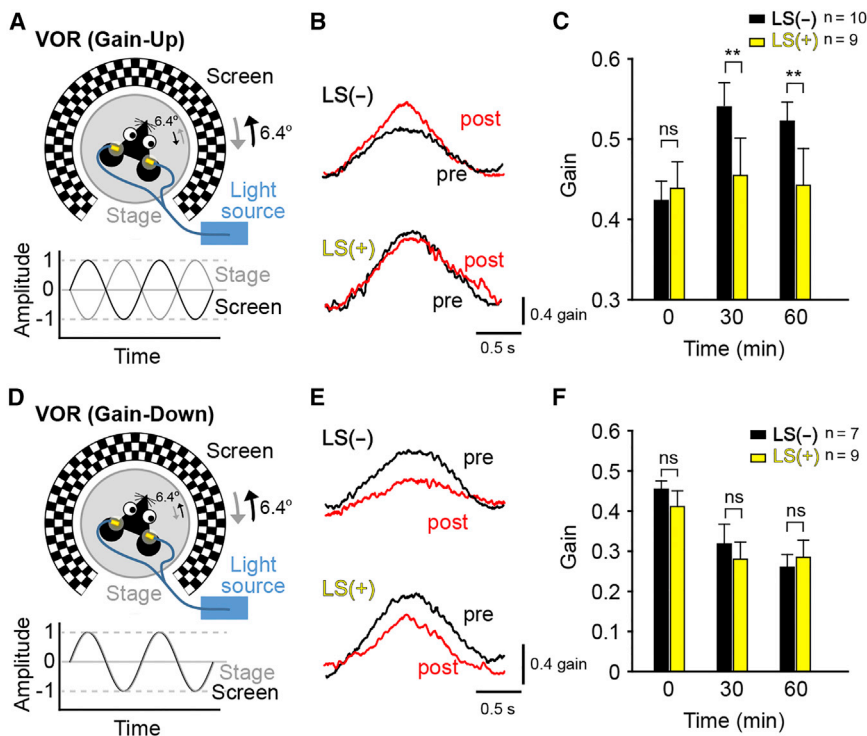
Data are presented as mean ± SEM.

Figure 7. Fiberoptic Illumination Inhibits VOR Adaptation in PC-PhotonSABER Mice

(A) Schematic drawing of the experimental setup. The PC-PhotonSABER mouse, which had optic fibers placed above bilateral flocculi, was surrounded by a checked-pattern optokinetic stimulation (screen). In the gain-up training, the screen was moved in the opposite direction (6.4 degrees and a frequency of 0.5 Hz) from the head.

(B) Representative VOR waveforms before (pre, black) and 60 min after (post, red) gain-up training without (LS[−], upper traces) and with (LS[+], lower traces) illumination.

(C) The time course of VOR gain adaptation in the gain-up protocol. The gain was measured before (0) and 30 and 60 min after training without (LS[−], n = 10 mice) or with (LS[+], n = 9 mice) light stimulation.

(D) In the gain-down protocol, the screen was moved in the same direction (6.4 degrees and a frequency of 0.5 Hz) as the head.

(E) Representative VOR waveforms before (pre, black) and 60 min after (post, red) gain-down training without (LS[−]) and with (LS[+]) illumination.

(F) The time course of VOR gain adaptation in the gain-down protocol. The gain was measured before (0) and 30 and 60 min after training without (LS[−], n = 7 mice) or with (LS[−], n = 9 mice) light stimulation.

**p < 0.001; ns, not significant; two-way ANOVA followed by Bonferroni post hoc test. Data are presented as mean ± SEM.

5B) without affecting basal synaptic transmission (Figure 4A) or other forms of synaptic plasticity, such as PF-LTP (Figures 4F and 5C) and RP of inhibitory synaptic inputs (Figure 4G), in acute slice preparations. Furthermore, fiberoptic illumination to the flocculi of PC-PhotonSABER mice inhibited cerebellar motor learning during adaptation of OKR (Figure 6) and VOR (Figure 7), as well as resulted in an AMPA receptor decrease in the flocculus in vivo (Figure 8). These results indicate that PF-LTD and AMPA receptor endocytosis are directly responsible for motor learning in vivo.

Essential Roles of PF-LTD and AMPA Receptor Endocytosis in Motor Learning

Establishing the functional role of LTD and AMPA receptor endocytosis in vivo has proven challenging due to a lack of selective tools (Collingridge et al., 2010; Yuzaki, 2013). For example, intraperitoneal administration of T-588, a pharmacological inhibitor of PF-LTD in vitro, was shown to block fast VOR adaptation in marmosets (Anzai and Nagao, 2014), but not in mice (Schonewille et al., 2011). While genetic engineering in mice assures cellular and molecular target specificity, compensatory mechanisms could modify synaptic plasticity in the remaining circuits and affect motor learning in vivo (Gao et al., 2012; Ito et al., 2014). For example, the RP of inhibitory synaptic inputs is proposed to compensate for the loss of PF-LTD by reducing Purkinje cell outputs (Hirano, 2014). In addition, the synaptic plasticity observed in mice, in which key synaptic molecules are genetically modified, does not necessarily reflect that of wild-type mice. Recently, cerebellar motor learning, as well as PF-LTP, but not PF-LTD, was shown to be impaired in mice lacking

GluA3 AMPA receptor subunits (Gutierrez-Castellanos et al., 2017). However, as basal synaptic excitatory transmission in GluA3-null Purkinje cells is reduced (Gutierrez-Castellanos et al., 2017), it remains unclear whether unusual subunit composition may affect the synaptic properties in these mice. Finally, another confounding factor is the various LTD induction protocols used in in vitro slice preparations (Suvrathan et al., 2016; Yamaguchi et al., 2016).

Unlike most pharmacological tools, PhotonSABER targets the final common step of LTD—the activity-dependent, clathrin-mediated rapid endocytosis of AMPA receptors (Collingridge et al., 2010; Huganir and Nicoll, 2013). Less active AMPA receptors or their constitutive recycling is unlikely to be affected, as was observed for normal basal synaptic transmission at PF- and CF-Purkinje cell synapses (Figures 4A and 4B). This finding is also consistent with recent reports showing that constitutive endocytosis of AMPA receptors is mediated by clathrin-independent pathways (Glebov et al., 2015; Zheng et al., 2015). Thus, PhotonSABER selectively inhibits activity-dependent endocytosis without relying on LTD induction protocols.

Unlike genetic manipulations, PhotonSABER achieved the rapid and reversible control of endocytosis in heterologous cells (Figure S1C) and neurons (Figure 1D). Light stimulus inhibited PF-LTD in a temporally controlled (Figure 4E) and reversible (Figure 4D) manner in PC-PhotonSABER slices. Unlike certain genetically modified mice, light stimulus did not affect PF-LTP (Figures 4F and 5C) or RP (Figure 4G) in PC-PhotonSABER slices. These results indicate that the compensatory pathways did not kick in when active endocytosis was rapidly and reversibly inhibited by PhotonSABER.
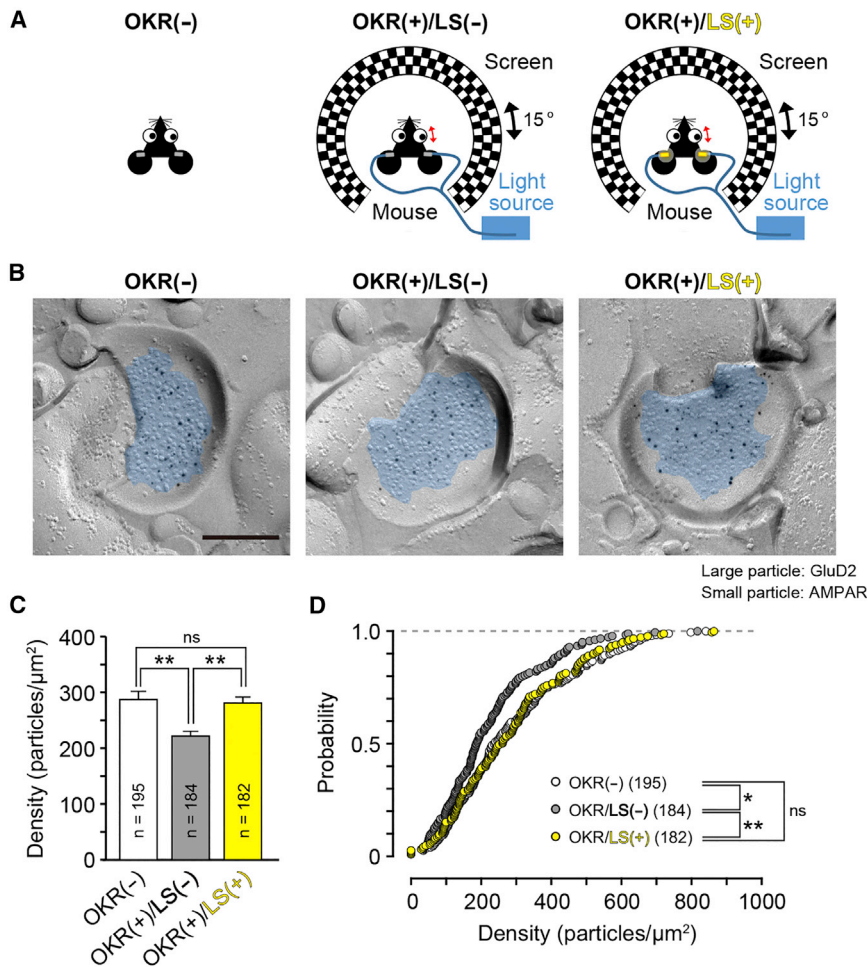
Figure 8. Fiberoptic Illumination Inhibits AMPA Receptor Endocytosis after OKR Adaptation in PC-PhotonSABER Mice

(A) Animals prepared for these experiments. Mice without (OKR[−], left) and with 60 min of OKR training in the absence (OKR[+]/LS[−], middle) and the presence (OKR[+]/LS[+], right) of light stimulation (LS). After OKR training, the density of AMPA receptors in the flocculus was analyzed using the SDS-FRL method.

(B) Representative photomicrographs showing the labeling for GluD2 (15-nm gold) and AMPA receptors (AMPAR: 5-nm gold) on freeze-fracture replicas from the flocculus of PC-PhotonSABER mice without (OKR[−]) and with 60 min of training under dark (OKR[+]/LS[−]) and light (OKR[+]/LS[+]) conditions. Scale bar, 200 nm.

(C and D) The graphs show the mean values (C) and cumulative distributions (D) of the AMPA receptor density at PF-Purkinje cell synapses in the flocculus. n = 3 mice for each condition. **p < 0.01 and *p < 0.05; ns, not significant; Kruskal-Wallis test followed by Scheffe post hoc test in (C) and Kolmogorov-Smirnov test in (D). Data are presented as mean + SEM.

X syndrome, Alzheimer's disease, drug addiction, and schizophrenia (Collingridge et al., 2010; Huganir and Nicoll, 2013). By mating *PhotonSABER-LSL* mice with cell-type-specific *Cre* driver mice, we can easily achieve cell-type-specific expression of PhotonSABER. Thus, by taking advantage of the acute control of AMPA receptor endocytosis, PhotonSABER is a powerful tool by which to clarify the direct roles of AMPA receptor endocytosis and LTD in various physiological and pathological functions at many synapses *in vivo*.

In addition to its high temporal control, another advantage of PhotonSABER is its reversibility. For example, delayed light stimulation did not inhibit PF-LTD (Figure 4E) or adaptation of OKR (Figure 6D) in PC-PhotonSABER mice. Furthermore, 10 min after the cessation of light, PF-LTD was normally induced in PC-PhotonSABER slices (Figure 4D). Although the acquisition, expression, and extinction phases of learning and memory are thought to be achieved by distinct synapses, the underlying molecular mechanisms are not completely clear. By taking advantage of the acute and reversible control of AMPA receptor endocytosis, PhotonSABER can be used to clarify the role of active AMPA receptor endocytosis at specific synapses during different phases of learning *in vivo*.

One caveat of using PhotonSABER is that it does not discriminate cargo proteins, but rather it affects active synapses undergoing increased endocytosis of any cargo. Indeed, PhotonSABER inhibited the endocytosis of dextran in HEK293 cells (Figure S2). Although PF-LTD in the cerebellum is likely caused by the selective endocytosis of AMPA receptors, other cargo proteins, such as NMDA receptors (NMDARs), are

PC-PhotonSABER inhibited PF-LTD induction in the flocculus *in vitro* (Figure 5B) and the adaptation of OKR *in vivo* (Figure 6C) in a similar time course. In addition, light stimulation inhibited the decrease in the synaptic AMPA receptor density in the flocculus associated with OKR (Wang et al., 2014) (Figures 8B–8D). Furthermore, light stimulation to the flocculus of PhotonSABER mice inhibited the adaptation of VOR in the gain-up, but not the gain-down, training (Figure 7), which is consistent with the proposed role of PF-LTD in the gain-up adaptation of VOR (Boyden et al., 2006). These results provide strong support for the causal role of AMPA receptor endocytosis and LTD at PF-Purkinje cell synapses in motor learning during OKR and VOR *in vivo*.

Advantages and Caveats of Using PhotonSABER

The major advantage of PhotonSABER is its high temporal and cell-type-specific control of LTD without affecting basal synaptic transmission or evoking compensatory synaptic plasticity. LTD and AMPA receptor endocytosis have been shown to occur at many synapses in various brain regions. In addition to its roles in learning and memory, LTD is thought to mediate the elimination of synapses in various brain regions during normal development and under pathological conditions, such as in fragile

endocytosed together with AMPA receptors in certain forms of LTD (Snyder et al., 2001). By taking advantage of the nonselective nature of cargo proteins, PhotonSABER could be used to characterize these forms of LTD. In addition, PhotonSABER could be used to determine the roles of activity-dependent endocytosis of other cargos, such as TrkB receptors for brain-derived neurotrophic factor.

The concept of optogenetically regulating active endocytosis by changing the luminal pH of early endosomes could be applied to other types of endosomes. For example, by targeting the photosensitive H^+ pumps to late endosomes/lysosomes and recycling endosomes, optogenetic control of autophagy (Colacurcio and Nixon, 2016) and LTP (Huganir and Nicoll, 2013; Malinow and Malenka, 2002) could be achieved, respectively, to elucidate their roles in various brain regions *in vivo*. Further development of optogenetic tools through the optimization of endosomal targeting and H^+ pump activity is warranted to regulate specific endosomal functions.

STAR★METHODS

Detailed methods are provided in the online version of this paper and include the following:

- KEY RESOURCES TABLE
- CONTACT FOR REAGENT AND RESORCE SHARING
- EXPERIMENTAL MODEL AND SUBJECT DETAILS
  - Mice
  - Primary Culture of Hippocampal and Cerebellar Neurons
- METHOD DETAILS
  - Construction of Plasmids
  - Immunofluorescence Analysis for Cultured Cells
  - Measurement of Endosomal pH
  - Assay for the Endosomal Localization of Dextran and AMPA Receptors
  - Antibody Feeding Assay for the AMPA Receptors
  - Chemical LTD in Hippocampal and Cerebellar Neurons
  - Immunoblot and Immunofluorescence Assays for Mouse Brain
  - Electrophysiology
  - Light Stimulation into Cerebella *In Vivo*
  - Eye Movement Measurements
  - SDS-Digested Freeze-Fracture Replica Labeling (SDS-FRL)
- QUANTIFICATION AND STATISTICAL ANALYSIS

SUPPLEMENTAL INFORMATION

Supplemental Information includes seven figures and can be found with this article online at https://doi.org/10.1016/j.neuron.2018.07.034.

A video abstract is available at http://dx.doi.org/10.1016/j.neuron.2018.07.034#mmc3.

AUTHOR CONTRIBUTIONS

W.K. performed electrophysiological analyses and VOR and OKR experiments, analyzed the data, and wrote the paper. A.K. performed and analyzed VOR experiments. S.N., K.K., and Y.F. carried out SDS-FRL experiments and analyzed data. E.M. and A.T. carried out immunocytochemical work. J.M. prepared knockin mice. S.M. designed the project, carried out the live imaging and biochemical and immunocytochemical works, generated knockin mice, analyzed the data, and wrote the paper. M.Y. designed and supervised the project and wrote the paper.

DECLARATION OF INTEREST

The authors declare no competing interests.

REFERENCES

Anzai, M., and Nagao, S. (2014). Motor learning in common marmosets: vestibulo-ocular reflex adaptation and its sensitivity to inhibitors of Purkinje cell long-term depression. Neurosci. Res. *83*, 33–42.

Boyden, E.S., Katoh, A., Pyle, J.L., Chatila, T.A., Tsien, R.W., and Raymond, J.L. (2006). Selective engagement of plasticity mechanisms for motor memory storage. Neuron *51*, 823–834.

Brown, T.C., Tran, I.C., Backos, D.S., and Esteban, J.A. (2005). NMDA receptor-dependent activation of the small GTPase Rab5 drives the removal of synaptic AMPA receptors during hippocampal LTD. Neuron *45*, 81–94.

Chen, T., Wang, W., Dong, Y.L., Zhang, M.M., Wang, J., Koga, K., Liao, Y.H., Li, J.L., Budisantoso, T., Shigemoto, R., et al. (2014). Postsynaptic insertion of AMPA receptor onto cortical pyramidal neurons in the anterior cingulate cortex after peripheral nerve injury. Mol. Brain *7*, 76.

Colacurcio, D.J., and Nixon, R.A. (2016). Disorders of lysosomal acidification-The emerging role of v-ATPase in aging and neurodegenerative disease. Ageing Res. Rev. *32*, 75–88.

Collingridge, G.L., Peineau, S., Howland, J.G., and Wang, Y.T. (2010). Long-term depression in the CNS. Nat. Rev. Neurosci. *11*, 459–473.

Crepel, F. (2007). Developmental changes in retrograde messengers involved in depolarization-induced suppression of excitation at parallel fiber-Purkinje cell synapses in rodents. J. Neurophysiol. *97*, 824–836.

De Zeeuw, C.I., and Ten Brinke, M.M. (2015). Motor learning and the cerebellum. Cold Spring Harb. Perspect. Biol. *7*, a021683.

Emi, K., Kakegawa, W., Miura, E., Ito-Ishida, A., Kohda, K., and Yuzaki, M. (2013). Reevaluation of the role of parallel fiber synapses in delay eyeblink conditioning in mice using Cbln1 as a tool. Front. Neural Circuits *7*, 180.

Fernández-Monreal, M., Brown, T.C., Royo, M., and Esteban, J.A. (2012). The balance between receptor recycling and trafficking toward lysosomes determines synaptic strength during long-term depression. J. Neurosci. *32*, 13200–13205.

Furuya, S., Makino, A., and Hirabayashi, Y. (1998). An improved method for culturing cerebellar Purkinje cells with differentiated dendrites under a mixed monolayer setting. Brain Res. Brain Res. Protoc. *3*, 192–198.

Gao, Z., van Beugen, B.J., and De Zeeuw, C.I. (2012). Distributed synergistic plasticity and cerebellar learning. Nat. Rev. Neurosci. *13*, 619–635.

Glebov, O.O., Tigaret, C.M., Mellor, J.R., and Henley, J.M. (2015). Clathrin-independent trafficking of AMPA receptors. J. Neurosci. *35*, 4830–4836.

Griffiths, G., Hoflack, B., Simons, K., Mellman, I., and Kornfeld, S. (1988). The mannose 6-phosphate receptor and the biogenesis of lysosomes. Cell *52*, 329–341.

Gutierrez-Castellanos, N., Da Silva-Matos, C.M., Zhou, K., Canto, C.B., Renner, M.C., Koene, L.M.C., Ozyildirim, O., Sprengel, R., Kessels, H.W., and De Zeeuw, C.I. (2017). Motor learning requires Purkinje cell synaptic potentiation through activation of AMPA-receptor subunit GluA3. Neuron 93, 409–424.

Hatanaka, T., Takeuchi, E., Katoh, A., Yamaki, T., Uchida, M., and Natsume, H. (2016). Preparation of bioadhesive phosphorescent particles and their use as markers for video-oculography of mice. Tokai J. Exp. Clin. Med. 41, 46–53.

Hirano, T. (2014). Around LTD hypothesis in motor learning. Cerebellum 13, 645–650.

Hoogenraad, C.C., Popa, I., Futai, K., Martinez-Sanchez, E., Wulf, P.S., van Vlijmen, T., Dortland, B.R., Oorschot, V., Govers, R., Monti, M., et al. (2010). Neuron specific Rab4 effector GRASP-1 coordinates membrane specialization and maturation of recycling endosomes. PLoS Biol. 8, e1000283.

Huganir, R.L., and Nicoll, R.A. (2013). AMPARs and synaptic plasticity: the last 25 years. Neuron 80, 704–717.

Huotari, J., and Helenius, A. (2011). Endosome maturation. EMBO J. 30, 3481–3500.

Ito, M., Yamaguchi, K., Nagao, S., and Yamazaki, T. (2014). Long-term depression as a model of cerebellar plasticity. Prog. Brain Res. 210, 1–30.

Kakegawa, W., and Yuzaki, M. (2005). A mechanism underlying AMPA receptor trafficking during cerebellar long-term potentiation. Proc. Natl. Acad. Sci. USA 102, 17846–17851.

Kakegawa, W., Mitakidis, N., Miura, E., Abe, M., Matsuda, K., Takeo, Y.H., Kohda, K., Motohashi, J., Takahashi, A., Nagao, S., et al. (2015). Anterograde C1ql1 signaling is required in order to determine and maintain a single-winner climbing fiber in the mouse cerebellum. Neuron 85, 316–329.

Kawanabe, A., Furutani, Y., Jung, K.H., and Kandori, H. (2009). Engineering an inward proton transport from a bacterial sensor rhodopsin. J. Am. Chem. Soc. 131, 16439–16444.

Kerr, M., and Teasdale, R.D. (2014). Live imaging of endosome dynamics. Semin. Cell Dev. Biol. 31, 11–19.

Kohda, K., Kakegawa, W., Matsuda, S., Yamamoto, T., Hirano, H., and Yuzaki, M. (2013). The δ2 glutamate receptor gates long-term depression by coordinating interactions between two AMPA receptor phosphorylation sites. Proc. Natl. Acad. Sci. USA 110, E948–E957.

Kozik, P., Hodson, N.A., Sahlender, D.A., Simecek, N., Soromani, C., Wu, J., Collinson, L.M., and Robinson, M.S. (2013). A human genome-wide screen for regulators of clathrin-coated vesicle formation reveals an unexpected role for the V-ATPase. Nat. Cell Biol. 15, 50–60.

Kreitzer, A.C., and Regehr, W.G. (2001). Retrograde inhibition of presynaptic calcium influx by endogenous cannabinoids at excitatory synapses onto Purkinje cells. Neuron 29, 717–727.

Lee, S.H., Liu, L., Wang, Y.T., and Sheng, M. (2002). Clathrin adaptor AP2 and NSF interact with overlapping sites of GluR2 and play distinct roles in AMPA receptor trafficking and hippocampal LTD. Neuron 36, 661–674.

Lee, S.H., Simonetta, A., and Sheng, M. (2004). Subunit rules governing the sorting of internalized AMPA receptors in hippocampal neurons. Neuron 43, 221–236.

Malinow, R., and Malenka, R.C. (2002). AMPA receptor trafficking and synaptic plasticity. Annu. Rev. Neurosci. 25, 103–126.

Martin, S.J., and Morris, R.G. (2002). New life in an old idea: the synaptic plasticity and memory hypothesis revisited. Hippocampus 12, 609–636.

Masugi-Tokita, M., and Shigemoto, R. (2007). High-resolution quantitative visualization of glutamate and GABA receptors at central synapses. Curr. Opin. Neurobiol. 17, 387–393.

Matsuda, S., Launey, T., Mikawa, S., and Hirai, H. (2000). Disruption of AMPA receptor GluR2 clusters following long-term depression induction in cerebellar Purkinje neurons. EMBO J. 19, 2765–2774.

Matsuda, S., Kakegawa, W., Budisantoso, T., Nomura, T., Kohda, K., and Yuzaki, M. (2013). Stargazin regulates AMPA receptor trafficking through adaptor protein complexes during long-term depression. Nat. Commun. 4, 2759.

Miesenböck, G., De Angelis, D.A., and Rothman, J.E. (1998). Visualizing secretion and synaptic transmission with pH-sensitive green fluorescent proteins. Nature 394, 192–195.

Nomura, T., Kakegawa, W., Matsuda, S., Kohda, K., Nishiyama, J., Takahashi, T., and Yuzaki, M. (2012). Cerebellar long-term depression requires dephosphorylation of TARP in Purkinje cells. Eur. J. Neurosci. 35, 402–410.

Ohtsuki, G., Kawaguchi, S.Y., Mishina, M., and Hirano, T. (2004). Enhanced inhibitory synaptic transmission in the cerebellar molecular layer of the GluRdelta2 knock-out mouse. J. Neurosci. 24, 10900–10907.

Padmashri, R., Reiner, B.C., Suresh, A., Spartz, E., and Dunaevsky, A. (2013). Altered structural and functional synaptic plasticity with motor skill learning in a mouse model of fragile X syndrome. J. Neurosci. 33, 19715–19723.

Schindelin, J., Arganda-Carreras, I., Frise, E., Kaynig, V., Longair, M., Pietzsch, T., Preibisch, S., Rueden, C., Saalfeld, S., Schmid, B., et al. (2012). Fiji: an open-source platform for biological-image analysis. Nat. Methods 9, 676–682.

Schonewille, M., Belmeguenai, A., Koekkoek, S.K., Houtman, S.H., Boele, H.J., van Beugen, B.J., Gao, Z., Badura, A., Ohtsuki, G., Amerika, W.E., et al. (2010). Purkinje cell-specific knockout of the protein phosphatase PP2B impairs potentiation and cerebellar motor learning. Neuron 67, 618–628.

Schonewille, M., Gao, Z., Boele, H.J., Veloz, M.F., Amerika, W.E., Simek, A.A., De Jeu, M.T., Steinberg, J.P., Takamiya, K., Hoebeek, F.E., et al. (2011). Reevaluating the role of LTD in cerebellar motor learning. Neuron 70, 43–50.

Schwake, M., Friedrich, T., and Jentsch, T.J. (2001). An internalization signal in ClC-5, an endosomal Cl-channel mutated in dent's disease. J. Biol. Chem. 276, 12049–12054.

Segev, N. (2011). Coordination of intracellular transport steps by GTPases. Semin. Cell Dev. Biol. 22, 33–38.

Snyder, E.M., Philpot, B.D., Huber, K.M., Dong, X., Fallon, J.R., and Bear, M.F. (2001). Internalization of ionotropic glutamate receptors in response to mGluR activation. Nat. Neurosci. 4, 1079–1085.

Sönnichsen, B., De Renzis, S., Nielsen, E., Rietdorf, J., and Zerial, M. (2000). Distinct membrane domains on endosomes in the recycling pathway visualized by multicolor imaging of Rab4, Rab5, and Rab11. J. Cell Biol. 149, 901–914.

Suvrathan, A., Payne, H.L., and Raymond, J.L. (2016). Timing rules for synaptic plasticity matched to behavioral function. Neuron 92, 959–967.

Tanaka, S., Kawaguchi, S.Y., Shioi, G., and Hirano, T. (2013). Long-term potentiation of inhibitory synaptic transmission onto cerebellar Purkinje neurons contributes to adaptation of vestibulo-ocular reflex. J. Neurosci. 33, 17209–17220.

Tukey, D.S., Ferreira, J.M., Antoine, S.O., D'amour, J.A., Ninan, I., Cabeza de Vaca, S., Incontro, S., Wincott, C., Horwitz, J.K., Hartner, D.T., et al. (2013). Sucrose ingestion induces rapid AMPA receptor trafficking. J. Neurosci. 33, 6123–6132.

Wadiche, J.I., and Jahr, C.E. (2005). Patterned expression of Purkinje cell glutamate transporters controls synaptic plasticity. Nat. Neurosci. 8, 1329–1334.

Wang, W., Nakadate, K., Masugi-Tokita, M., Shutoh, F., Aziz, W., Tarusawa, E., Lorincz, A., Molnár, E., Kesaf, S., Li, Y.Q., et al. (2014). Distinct cerebellar engrams in short-term and long-term motor learning. Proc. Natl. Acad. Sci. USA 111, E188–E193.

Xia, J., Chung, H.J., Wihler, C., Huganir, R.L., and Linden, D.J. (2000). Cerebellar long-term depression requires PKC-regulated interactions between GluR2/3 and PDZ domain-containing proteins. Neuron 28, 499–510.

Yamaguchi, K., Itohara, S., and Ito, M. (2016). Reassessment of long-term depression in cerebellar Purkinje cells in mice carrying mutated GluA2 C terminus. Proc. Natl. Acad. Sci. USA 113, 10192–10197.

Yuzaki, M. (2013). Cerebellar LTD vs. motor learning-lessons learned from studying GluD2. Neural Netw. 47, 36–41.

Zheng, N., Jeyifous, O., Munro, C., Montgomery, J.M., and Green, W.N. (2015). Synaptic activity regulates AMPA receptor trafficking through different recycling pathways. eLife 4, e06878.

Zucker, R.S., and Regehr, W.G. (2002). Short-term synaptic plasticity. Annu. Rev. Physiol. 64, 355–405.

STAR★METHODS

KEY RESOURCES TABLE

REAGENT or RESOURCE	SOURCE	IDENTIFIER
Antibodies		
Mouse monoclonal anti-HA	Covance	MMS-101P; RRID: AB_ 2314672
Rat monoclonal anti-HA	Roche	11 867 423 001; RRID: AB_390918
Rabbit polyclonal anti-HA	MBL international	561; RRID: AB_591839
Rabbit polyclonal anti-FLAG	Sigma-Aldrich	F7425;RRID: AB_439687
Rabbit polyclonal anti-Calbindin-D28K	Sigma-Aldrich	C2724; RRID: AB_258818
Guinea pig polyclonal anti-Calbindin-D28K	Frontier Institute	Calbindin-GP-Af280; RRID: AB_2571570
Mouse monoclonal anti-Mannose 6 Phosphate Receptor antibody	Novus Biologicals	NB300-514; RRID: AB_531523
Rabbit monoclonal anti-CD71 (Transferrin Receptor) antibody	Cell Signaling Technology	13113; RRID: AB_2715594
Rabbit polyclonal anti-LAMP1 antibody	Sigma-Aldrich	L1418; RRID: AB_477157
Mouse monoclonal anti-actin	Sigma-Aldrich	A3853,; RRID: AB_262137
Rabbit polyclonal anti-early endosome antigen (EEA) 1 antibodies	Millipore	07-1820; RRID: AB_10615480
Mouse monoclonal anti-MAP2A,2B	Millipore	MAB378; RRID: AB_94967
Alexa546 goat anti-rat IgG	Thermo Fisher Scientific	A-11081; RRID: AB_2534125
Alexa546 goat anti-mouse IgG	Thermo Fisher Scientific	A-11003; RRID: AB_2534071
Alexa546 goat anti-rabbit IgG	Thermo Fisher Scientific	A-11010; RRID: AB_2534077
Alexa488 goat anti-rabbit IgG	Thermo Fisher Scientific	A-11008; RRID: AB_143165
Alexa405 goat anti-mouse IgG	Thermo Fisher Scientific	A-31553; RRID: AB_221604
Alexa350 goat anti-mouse IgG	Thermo Fisher Scientific	A-11045; RRID: AB_2534100
Goat anti-Rabbit IgG, HRP-conjugated	Millipore	12-348; RRID: AB_390191
Goat anti-rat IgG, HRP-conjugated	Millipore	AP136P; RRID: AB_11214444
Goat anti-mouse IgG, HRP-conjugated	Millipore	12-349; RRID: AB_390192
Chemicals, Peptides, and Recombinant Proteins		
NMDA	Tocris Bioscience	0114
D-AP5	Tocris Bioscience	0106
NBQX	Tocris Bioscience	0373
SCH50911	Tocris Bioscience	0984
QX-314	Tocris Bioscience	1014
Tetrodotoxin	Alomone Labs	T-550
Picrotoxin	Sigma-Aldrich	P1675
TPA	Sigma-Aldrich	P1585
Monensin	Sigma-Aldrich	M5273
Nigericin	Sigma-Aldrich	N7143
Recombinant Botulinum neurotoxin Type A light chain	R&D Systems	4489-ZN
pHrodo-Dextran	Thermo Fisher Scientific	P10361
Critical Commercial Assays		
Lipofectamine 2000	Thermo Fisher Scientific	11668027
Experimental Models: Cell Lines		
HEK293tSA Cells	Dr. R. Horn (Thomas Jefferson Univ., PA)	N/A
COS-7 Cells	ATCC	CRL-1651

(*Continued on next page*)

Continued

REAGENT or RESOURCE	SOURCE	IDENTIFIER
Experimental Models: Organisms/Strains		
Mouse: Wild-type (C57BL/6J)	Japan SLC	C57BL/6J
Mouse:PhotonSABER-LSL	This paper	N/A
Mouse:PC-PhotonSABER	This paper	N/A
Recombinant DNA		
pCAGGS PhotonSABER-FLAG	This paper	N/A
pcDNA SEP PhotonSABER	This paper	N/A
pCAGGS HA-GluA2	Matsuda et al., 2013	N/A
pCAGGS HA-GluA2	Matsuda et al., 2013	N/A
pCAGGS HA-GluA2	Matsuda et al., 2013	N/A
pCAGGS HA-GluA2	Matsuda et al., 2013	N/A
Software and Algorithms		
IPLab	Scanalytics	https://spectraservices.com/IPLAB.html; RRID: SCR_002775
pClamp	Molecular Devices	https://www.moleculardevices.com/products/axon-patch-clamp-system/acquisition-and-analysis-software/pclamp-software-suite
Fiji	NIH	https://fiji.sc/RRID: SCR_002285
MATLAB	MathWorks	https://www.mathworks.com/products/matlab.html; RRID: SCR_001622
Sigma Plot	Systat Software	https://systatsoftware.com/products/sigmaplot/; RRID: SCR_003210
BellCurve for Excel	Social Survey Research Information	https://bellcurve.jp/
Adobe Photoshop	Adobe	https://www.adobe.com/products/photoshop.html; RRID: SCR_014199
Adobe Illustrator	Adobe	https://www.adobe.com/products/illustrator.html; RRID: SCR_014198

CONTACT FOR REAGENT AND RESORCE SHARING

Further information and requests for resources and reagents should be directed to the Lead Contact Michisuke Yuzaki (myuzaki@keio.jp).

EXPERIMENTAL MODEL AND SUBJECT DETAILS

Mice

All procedures related to animal care and treatment were performed in accordance with the guidelines approved by the animal resource committees of the University of Electro-communications and Keio University. Mice were housed with a 12:12 h light-dark cycle with food and water available *ad libitum*. PC-PhotonSABER mice at postnatal 8 to 10 weeks were subjected to adaptation of horizontal optokinetic response (OKR) and vestibule-ocular reflex (VOR).

Primary Culture of Hippocampal and Cerebellar Neurons

Hippocampal cultures were prepared as described previously (Matsuda et al., 2013). Briefly, hippocampi dissected from embryonic days (E) 16−17 ICR mice were digested using 10 U/ml trypsin and 100 U/ml DNase at 37°C for 20 min. The dissociated hippocampal neurons were plated at a density of 2X10^5 cells on polyethyleneimine-coated glass coverslips (diameter, 13.5 mm), and were cultured in neurobasal medium (Invitrogen) with NS21 supplement and 0.5 mM ʟ-glutamine. At 7−10 days *in vitro*, neurons were transfected with plasmids using LipofectAMINE 2000 (Invitrogen), and used for the assay of AMPA receptor endocytosis.

Cerebellar cultures were prepared from E16−17 ICR mice by modifying a reported method (Furuya et al., 1998). Cells were plated at a density of 2X10^5 cells on glass coverslips (diameter, 13.5 mm) and were maintained in DMEM/F12 (Invitrogen) containing 100 µM putrescine, 30 nM sodium selenite, 0.5 ng∕mL Tri-iodothyronine (Sigma-Aldrich), 3.9 mM ʟ-glutamate (Invitrogen) and N3

supplement (100 μg/mL apo-transferrin, 10 μg/mL insulin, and 20 nM progesterone; all from Sigma-Aldrich) with 1% fetal calf serum in 5% CO_2 at 37°C. At 7−10 days *in vitro*, neurons were transfected with plasmids using Amaxa Nucleofector (Lonza, Basel, Switzerland), and used for the assay of AMPA receptor endocytosis.

METHOD DETAILS

Construction of Plasmids

The cDNA encoding ASR (GenBank: WP_010997316.1; with Asp217 replaced by Glu) with codon optimization for mouse was synthesized by Takara Bio. To generate a cDNA encoding photonSABER, the cDNA encoding C-terminal intracellular region of ASR (from His219 to the end) was replaced with the C-terminal region of mouse chloride channel protein 5 (Clcn5, GeneBank: NP_001230691.1; from Asp565 to the end). The cDNAs encoding SEP and FLAG tag was added to the 5′ end (immediately following the signal sequence) and 3′ end (immediately upstream of the stop codon) of PhotonSABER, respectively. The cDNA encoding an HA tag was added to the 5′ end (immediately following the signal sequence) of mouse GluA2. The nucleotide sequences of the amplified open reading frames were confirmed by bidirectional sequencing. The cDNAs encoding GFP-tagged Rab4, Rab7 and Rab11 were kindly provided by Dr. Fukuda (Tohoku University, Sendai, Japan). After the cDNAs were cloned into pcDNA (Invitrogen) or pCAGGS (kindly provided by Dr. J Miyazaki, Osaka University, Osaka, Japan) vectors, the constructs were transfected into HEK293 cells (tSA, kindly provided by Dr. R Horn, Thomas Jefferson University, Philadelphia, PA) using the calcium phosphate method.

Immunofluorescence Analysis for Cultured Cells

HEK293 cells or cultured hippocampal neurons expressing PhotonSABER-FLAG and GFP-tagged Rab proteins were fixed using 4% paraformaldehyde (PFA) in phosphate-buffered saline (PBS) for 10 min at room temperature. After washing with PBS for three times, cells were blocked with PBS containing 2% bovine serum albumin, 2% normal goat serum, and 0.4% Triton X-100. To label for PhotonSABER-FLAG, cells were incubated with anti-FLAG antibodies (1:300) for 1 h and visualized with Alexa546 secondary antibody (1:1000; Invitrogen). In the representative images, brightness and contrast were adjusted uniformly within each experimental series for consistent visibility. For the colocalization assay in hippocampal neurons, the fluorescence intensities of GFP (Rab) and Alexa546 (PhotonSABER) were quantified along the region of interest (ROI) set on dendrites using an IP-Lab software (Scanalytics). Local maximal points, which had more than twice the average fluorescence signals in the ROI, were identified by eye and defined as peaks. We defined that PhotonSABER and Rab overlapped with each other when more than half of each peak fluorescence signal was observed at the same position. The percentage of Alexa546 peaks colocalized with GFP was calculated.

Measurement of Endosomal pH

HEK293 cells, COS-7 cells or hippocampal neurons expressing SEP-tagged PhotonSABER were incubated with dextran-conjugated pHrode (Molecular Probes) for 10 min. After changing the medium to the imaging solution (in mM): 25 HEPES, 140 NaCl, 5 KCl, 1.3 $CaCl_2$, 33 D-glucose; pH 7.0), which contained 10 mM nocodazole to inhibit endosome movements, the fluorescence images of living cells under dark conditions were captured with confocal microscopes (Olympus FV1200 for HEK293 and COS cells and Olympus CSU-W1 for hippocampal neurons). Subsequently, the cells were stimulated with light (central wavelength = 575 nm, wavelength width = 25 nm) and the images were captured at various time points. On completion of live imaging, the imaging solution was changed to various pH calibration solutions (pH 5.0, 5.8, 6.5, and 7.5) containing H^+-ionophores (10 μM monensin and 10 μM nigericin (both from Sigma-Aldrich). The fluorescence intensities of SEP and pHrode in endosomes (defined as SEP- and pHrode-double positive regions) were measured by using Fiji software (Schindelin et al., 2012). The ratio of SEP/pHrode at pH = 5.8 was established to 100%.

Assay for the Endosomal Localization of Dextran and AMPA Receptors

To visualize late endosomes, HEK293 cells expressing GFP-tagged Rab7 and PhotonSABER-FLAG were incubated with biotinylated dextran for 2 min or 60 min in the presence of light stimulations at the various illuminance (0−10^5 lux). After fixation with 4% PFA, dextran incorporated into endosomes was visualized by Alexa546-conjugated streptavidin (Molecular Probes). The fluorescence images were captured by confocal microscope and the intensities of Alexa546 on the GFP positive region was quantified by using IPlab software.

To visualize AMPA receptors in early endosomes in cultured hippocampal neurons, 50 μM NMDA (Tocris Bioscience) was applied to hippocampal neurons expressing HA-GluA2, GFP-tagged Rab4 and PhotonSABER-FLAG. Three min after the stimulation, cells were fixed with 4% PFA and the localization of HA-GluA2 and PhotonSABER-FLAG were visualized by immunostaining using anti-HA (mouse, 1:1000) and anti-FLAG (1:300) antibodies. Anti-HA, and anti-FLAG antibodies were detected by Alexa546- and Alexa405-conjugated secondary antibodies (Molecular Probes), respectively. The fluorescence images were captured by confocal microscope and the fluorescence intensities of Alexa546 on the GFP-positive regions in the dendrites were measured and normalized by total Alexa546 fluorescence intensities within the dendrites. The mean values of control neurons were established as 100%.

To visualize AMPA receptors in endosomes in cultured Purkinje cells, 1 μM TPA (Sigma-Aldrich) was applied to Purkinje neurons expressing HA-GluA2 and PhotonSABER-FLAG. Three min (for EEA1 and TfR) or 20 min (for M6PR) after the stimulation, cells were

fixed and the localization of HA-GluA2 and endosome markers were visualized by immunostaining using anti-HA mouse (1:1000) or rabbit (1:500), anti-endosome markers (EEA1 1:200, M6PR 1:100, TfR 1:100) and anti-Calbindin rabbit (1:500) or guinea pig (1:200) antibodies. Anti-HA, anti-endosome marker, anti-Calbindin antibodies were detected by Alexa405-, Alexa546- and Alexa488-conjugated secondary antibodies (Molecular Probes), respectively. The fluorescence images were captured by confocal microscope and the intensities of Alexa405 fluorescence on the Alexa488-positive regions in the dendrites were measured and normalized by the total Alexa405 fluorescence intensities within the dendrites. The mean values of control neurons were established to 100%. Brightness and contrast were adjusted uniformly within each experimental series in the representative images.

Antibody Feeding Assay for the AMPA Receptors

Living cultured hippocampal neurons expressing HA-GluA2 and PhotonSABER-FLAG were labeled with anti-HA mouse antibodies (1:100). To induce chemical LTD, 50-μM NMDA was applied to hippocampal neurons for 3 min. After excess amount of antibodies were washed out by ice-cold PBS, cells were fixed with 4% PFA, washed twice with PBS and incubated with a blocking solution (2% BSA and 2% normal goat serum in PBS). Cell surface anti-HA antibodies were detected by Alexa546-conjugated secondary antibody (1:1000). Cells were then permeabilized with 0.4% Triton X-100 in a blocking solution and internalized anti-HA antibodies were detected by Alexa488-secondary antibody (1:1000). Expression of PhotonSABER-FLAG in cultured hippocampal neurons was also detected by anti-FLAG antibody (1:300) and Alexa350-secondary antibody. Fluorescence images were captured by a fluorescence microscope (BX60, Olympus) equipped with a CCD camera (DP70, Olympus) and analyzed using IP-Lab software (Scanalytics). In the representative images, brightness and contrast were adjusted uniformly for consistent visibility. For statistical analysis of the internalized HA-GluA2, the intensity of Alexa488 was measured and normalized using the intensity of Alexa546 for surface HA-GluA2. The fluorescence intensity of dendrites between 30 and 100 μm from the soma was measured.

Chemical LTD in Hippocampal and Cerebellar Neurons

Cultured hippocampal and cerebellar neurons were transfected with plasmids encoding HA-GluA2 and PhotonSABER-FLAG. To induce chemical LTD, 50-μM NMDA was applied to hippocampal neurons for 10 min and 1 μM TPA (Sigma-Aldrich) was applied to cerebellar neurons for 20 min in the presence of light stimulations ($0-10^5$ lux). Cells were fixed with 4% PFA, washed twice with PBS, and incubated with a blocking solution (2% BSA and 2% normal goat serum in PBS). Cell surface HA-GluA2 was labeled with the anti-HA antibody (1:1000), and visualized with Alexa546-secondary antibody (1:1000). Cells were then permeabilized with 0.4% Triton X-100 in a blocking solution and total HA-GluA2 was labeled with the anti-HA (1:1000) and Alexa350-secondary antibody (1:1000). Expression of PhotonSABER-FLAG in cultured hippocampal neurons was also detected by anti-FLAG (1:300) and Alexa488-secondary antibody (1:1000). Cerebellar Purkinje cells were identified with anti-Calbindin-D28K (1:500) and Alexa488-secondary antibody. Fluorescence images were captured by a fluorescence microscope (BX60, Olympus) equipped with a CCD camera (DP70, Olympus) and analyzed using IP-Lab software (Scanalytics). In the representative images, brightness and contrast were adjusted uniformly within each experimental series for consistent visibility. Heatmaps were generated by using Fiji image processing software. For statistical analysis of the surface expression level of HA-GluA2, the intensity of Alexa546 for surface HA-GluA2 was measured and normalized using the intensity of Alexa350 for total HA-GluA2. The fluorescence intensity of dendrites between 30 and 100 μm from the soma was measured.

To determine the wavelength dependency, various wavelengths of light were applied through band-pass filters (Cyan, 475/28 nm for center wavelength/full width at half maximum; Green, 542/27 nm; Yellow, 575/25 nm; Infrared, 850/50 nm) to cultured hippocampal neurons expressing HA-GluA2 and PhotonSABER during chemical LTD induction stimulus. To examine the effect of focal light stimulation, part of the dendrites of hippocampal neurons expressing HA-GluA2 and PhotonSABER-FLAG was stimulated by confocal laser (wavelength 561nm, Olympus CSU-W1) during chemical LTD induction stimulus.

Immunoblot and Immunofluorescence Assays for Mouse Brain

For immunoblot analysis, the cerebrum or cerebellum of the wild-type and PC-PhotonSABER mice were solubilized in 500 μL of TNE buffer (50 mM NaCl, 10% NP-40, 20 mM EDTA, 0.1% SDS, 50 mM Tris-HCl, pH 8.0) supplemented with a protease inhibitor cocktail (Calbiochem). After centrifugation, the supernatant was analyzed using immunoblotting with anti-HA rat, anti-Calbindin-D28K, anti-actin antibodies and HRP-conjugated secondary antibody, and chemiluminescent HRP substrate (Immobilon, Millipore).

For immunofluorescence assay, 100-μm thick cerebellar slices, prepared from the wild-type or PC-PhotonSABER mice, were incubated in the blocking solution containing 0.4% Triton X-100, and incubated with anti-HA rat (1: 1000) or rabbit (1:500) antibodies and anti-Calbindin-D28K (1:500) or anti-EEA1 (1:200) or anti-TfR (1:100) or anti-LAMP1 (1:200) rabbit antibodies or anti-M6PR (1:100) mouse antibodies. Anti-HA antibodies were detected by Alexa546-conjugated secondary antibodies and anti-Calbindin-D28K, EEA1, M6PR, TfR, LAMP1 antibodies were detected by Alexa488-conjugated secondary antibodies. To quantify colocalization of PhotonSABER with endosomes, the intensities of Alexa546 fluorescence on endosomes (defined as Alexa488-positive regions) were measured by using IPlab software and normalized by total Alexa546 fluorescence intensities. In the representative images, brightness and contrast were adjusted for consistent visibility.

Electrophysiology

Acute cerebellar slices were prepared from the vermis (sagittal section, 200 μm in thickness) and the hemisphere with flocculus (coronal section, 200 μm in thickness) of PC-PhotonSABER mice (postnatal day 14−42), as described previously (Kakegawa et al., 2015). Whole-cell patch-clamp recordings were made from visually identified Purkinje cells using a 60 X water-immersion objective attached to an upright microscope (BX51WI, Olympus) at room temperature. The solution used for slice storage and recording consisted of the following (in mM): 125 NaCl, 2.5 KCl, 2 $CaCl_2$, 1 $MgCl_2$, 1.25 NaH_2PO_4, 26 $NaHCO_3$ and 10 D-glucose, bubbled continuously with a mixture of 95% O_2 and 5% CO_2. For EPSC recordings, picrotoxin (100 μM, Sigma-Aldrich) was always present in the saline to block the inhibitory inputs. Intracellular solutions were composed of (in mM): 65 Cs-methanesulfonate, 65 K-gluconate, 20 HEPES, 10 KCl, 1 $MgCl_2$, 4 Na_2ATP, 1 Na_2GTP, 5 sucrose, and 0.4 EGTA (pH 7.25, 295 mOsm/kg) for PF-EPSC recordings and PF-LTD experiments (Kakegawa et al., 2015); 130 K-gluconate, 10 KCl, 10 HEPES, 1 $MgCl_2$, 4 Na_2ATP, 1 Na_2GTP, 16 sucrose (pH 7.25, 295 mOsm/kg) for PF-LTP experiments (Emi et al., 2013); 150 Cs-gluconate, 10 HEPES, 4 $MgCl_2$, 4 Na_2ATP, 1 Na_2GTP, 0.4 EGTA and 5 lidocaine N-ethyl bromide (QX-314; Tocris Bioscience) (pH 7.25, 292 mOsm/kg) for CF-EPSC and miniature EPSC (mEPSC) recordings (Kakegawa et al., 2015); 150 CsCl, 15 CsOH, 0.5 EGTA, 10 HEPES, 2 Na_2-ATP, 0.2 Na_2GTP (pH 7.3, 290 mOsm/kg) for RP experiments (Ohtsuki et al., 2004). The patch pipette resistance was 1.5−3 MΩ when filled with each intracellular solution. We kept the slices in the dark conditions (∼0 lux) for at least 10 min before visually guided patching to prevent any possible activation of PhotonSABER. During recordings, the slices were kept in the dark or light conditions by delivering light from the epifluorescence port and through the objective (central wavelength = 575 nm, wavelength width = 25 nm, power intensity at the tip of a 60X objective = 2.5−3.0 mW; SPECTRA X light engine, lumencor). Ambient room light (70–100 lux) does not significantly affect PF-LTD induction (Figure S7), indicating that neurons expressing PhotonSABER in slice preparations under the microscope may not be effectively activated by ambient room light.

To evoke CF- and PF-EPSCs, square pulses were applied through a stimulating electrode placed on the granular layer (10 μs, 100−200 μA) and the molecular layer (∼50 μm away from the pial surface; 10 μs, 100−200 μA), respectively. Selective stimulation of CFs and PFs was confirmed with the paired-pulse depression and paired-pulse facilitation of EPSC amplitudes at a 50-ms inter-stimulus interval, respectively. In the mEPSC recordings, 1 μM tetrodotoxin (a Na^+ channel blocker; Alomone Labs) was applied to the extracellular solution during recordings. mEPSC traces were analyzed by using a MINI ANALYSIS program (Synaptosoft) and observed events < 10 pA were discarded. Spontaneous firing patterns in Purkinje cells were examined by cell-attached recordings, obtained in voltage-clamp mode at room temperature.

For LTD experiments, PF-EPSCs were evoked at 0.1 Hz from Purkinje cells voltage-clamped at −80 mV. After stable PF-EPSCs were observed for at least 10 min, a conjunctive stimulation (CJ-stim), composed of 30 single PF stimuli and 200-ms depolarizing pulses (from −60 to +20 mV), was applied to induce LTD (Kohda et al., 2013). In some LTD recordings from flocculus, 100 nM bot-ulinum neurotoxin Type A light chain ($BoNT^{LC}$; R&D systems) was loaded into a Purkinje cell through a patch pipette to suppress AMPA receptor exocytosis (Kakegawa and Yuzaki, 2005). For induction of postsynaptic LTP, 300 times of PF stimuli were applied at a frequency of 1 Hz in the current-clamp mode (Emi et al., 2013). In the RP experiments, miniature inhibitory postsynaptic current (mIPSC) was measured from Purkinje cells clamped at −70 mV in the presence of 10 μM 2,3-dioxo-6-nitro-1,2,3,4-tetrahtdrobenzo[f] quinoxaline-7-sulfonamide disodium salt (NBQX; an AMPA receptor/kainate receptor antagonist; Tocris Bioscience), 50 μM D-AP5 (an NMDA receptor antagonist; Tocris Bioscience), 20 μM SCH50911 (a $GABA_B$ receptor antagonist; Tocris Bioscience) and 1 μM tetrodotoxin (a Na^+ channel blocker; Alomone Labs) in the external solution. For induction of the RP, a conditioning stimulation con-sisting of 5 trains of depolarization of Purkinje cells (500-ms pulses from −70 mV to −20 mV at 0.5 Hz) was applied (Ohtsuki et al., 2004). Access resistances were monitored every 10 s and 5 min for LTD/LTP and RP experiments, respectively, by measuring the peak currents in response to 2-mV, 50-ms hyperpolarizing steps throughout the experiments; the measurements were discarded if the resistance changed by more than 20% of its original value. Current responses were recorded with an Axopatch 200B amplifier (Molecular Devices), and pClamp software (version 9.2, Molecular Devices) was used for data acquisition and analysis. Signals were filtered at 1 kHz and digitized at 4 kHz for the EPSCs, and 10 kHz for the mEPSCs, mIPSCs and the spike recordings.

Light Stimulation into Cerebella *In Vivo*

PC-PhotonSABER mice at postnatal 8 to 10 weeks were anesthetized with an intraperitoneal injection of ketamine/xylazine (80/20 mg/kg; Sigma-Aldrich) and a 1-cm flat-head screw was attached to the cranial bone with synthetic resin cement (Super-Bond, Sun Medical). Subsequently, a small hole was made on the periotic capsule bilaterally using dental drill and cannulae were implanted above the hole using synthetic resin cement to allow access to the cerebellar flocculi. Several days later, mice were placed on a table with their head fixed with a screw and the body loosely strained in a plastic cylinder. Then, bifurcated optical fibers (1.25 mm diameter, branching fiber-optic patch cords, Doric Lenses) were inserted into cannulae to apply light stimulation to both flocculi. For fiberoptic illumination, light (central wavelength = 575 nm, wavelength width = 25 nm; SPECTRA X light engine) was delivered to the open ends of the optical fibers (power intensity at the output tip was ∼8 mW). In a control experiment, fiberoptic illumination was applied to the vermis of PC-PhotonSABER mice.

Eye Movement Measurements

OKR was measured using a sinusoidal oscillation of the checked-pattern screen (screen height, 55 cm from the eye of the mouse; check size, 2-cm square) by 15° (peak-to-peak) at various frequencies (0.1, 0.2, 0.33, 0.5 and 1.0 Hz). For OKR adaptation

experiment, the screen was moved repeatedly at 0.33 Hz for 1 h in light (300−400 lux). Over 10 cycles of the evoked eye movements free from blinks and saccades were averaged, and the mean amplitude was calculated using a modified Fourier analysis as previously described (Kakegawa et al., 2015). The gain of the eye movement was defined as the ratio of the peak-to-peak amplitude of eye movements to that of the screen oscillation.

VOR measurement was performed as previously described (Hatanaka et al., 2016). Briefly, the horizontal VOR was induced under the dark condition by applying turntable rotations about an earth-vertical axis, with a sinusoidal angular velocity of frequency 0.5 Hz, amplitude of 6.4° (peak-to-peak) and peak speed of 10°/s. Before VOR measurements, one drop (∼1 μl) of ophthalmic solution containing 1% pilocarpine hydrochloride (Sanpilo, Santen) was applied on the right eye of the mouse using a blunt needle. The pupil was tracked by an automated target tracking program (Move-tr/2D, Library). The artifacts caused by saccadic eye motion and eye blinking were removed from the acceleration data by the thresholding method using MATLAB (Mathworks, Natick, MA). The VOR gain was calculated as the ratio of the eye velocity amplitude to the head (turntable) velocity amplitude after fitting them to a sine curve at the fundamental stimulus frequency, 0.5 Hz, using a nonlinear least-squares regression program using MATLAB. We induced the adaptive motor learning in the VOR by pairing head rotation with rotation of the optokinetic stimulation projected on the inside wall of the cylinder placed around the restrainer of a mouse. The gain-up stimulus consisted of 0.5 Hz, 10°/s peak velocity, sinusoidal turntable rotation paired with oppositely directed 10°/s, sinusoidal visual rotation (with both speeds measured relative to the external world). For the gain-down training, the visual stimulation was held stationary relative to the mouse, while 0.5 Hz, 10°/s sinusoidal turntable rotation was delivered as well as gain-up protocol. At the beginning and each 30-min block of training, the VOR was measured in darkness with 0.5 Hz, 10°/s sinusoidal turntable rotation. Light stimulation to flocculi was applied during training and its illumination was stopped during VOR measurement.

SDS-Digested Freeze-Fracture Replica Labeling (SDS-FRL)

Adult PC-PhotonSABER mice (8−10 weeks, n = 3 mice for each condition) were perfused transcardially with 0.5% PFA and 15% saturated picric acid in 0.1 M phosphate buffer (pH 7.2), and 3 replicas of the cerebellum from individual mice were prepared and immunolabeled with anti-pan-AMPA receptor and anti-GluD2 antibodies (guinea pig) as described previously (Wang et al., 2014). Labeled replicas were investigated with a Tecnai 12 transmission electron microscope. The exoplasmic (E) faces of replicated plasma membranes with clusters of intramembrane particles (IMP) labeled with immunogold particles for GluD2 were considered as PF−Purkinje cell synapses and photomicrographed with a CCD digital camera at a magnification of 97,000X. The area of postsynaptic membrane specializations was measured by demarcating the outline of the IMP clusters, and the number of immuno-gold particles was counted using iTEM software. All particles within 20 nm from the outside edge of the E-face IMP cluster were counted as synaptic labeling because they can be distant from the epitope. The EM images were calibrated using a calibration grid. Specificity of the anti- AMPA receptor and anti-GluD2 antibodies was confirmed previously (Wang et al., 2014) and background labeling assessed on the P-face of presynaptic profiles in the present study was of negligible level.

QUANTIFICATION AND STATISTICAL ANALYSIS

Statistical methods were not used to predetermine the sample size. The experiments were not randomized. Data are presented as the mean ± SEM or mean + SEM. All tests were performed with Sigma Plot (Systat software) or BellCurve for Excel (Social Survey Research Information). For the comparison between two groups, we used two-tailed Student's t test, Mann-Whitney U test, Wilcoxon signed-rank test or Kolomogorov-Smirnov test unless stated otherwise. For the comparison among several groups, analyses of variance (ANOVA) or Kruskal-Wallis test, followed by the post hoc tests, was used. $p < 0.05$ was considered statistically significant.